Toward a Shock Grammar for Recognition

Kaleem Siddiqi [1] and Benjamin B. Kimia [2]

September 1995

[1]siddiqi@cim.mcgill.ca; McGill University, Center for Intelligent Machines.
[2]kimia@lems.brown.edu; Brown University, Laboratory for Engineering Man/Machine Systems.

Contents

Toward a Shock Grammar for Recognition

Kaleem Siddiqi and Benjamin B. Kimia

Abstract The recognition of objects from their projected two-dimensional shapes is a challenging problem owing to the spectrum of possible variations reflected in the image domain, *e.g.*, those caused by movement of parts, changes in viewing geometry, occlusion, *etc.* This motivates a need for quantitative as well as qualitative descriptions of shape in terms of structural relations between components; the latter remain largely invariant under the above changes. In this paper we confront the theoretical and practical difficulties of computing such a representation, based on the detection of *shocks* or singularities that arise as a shape is deformed, as organized in two stages. First, we develop subpixel *local* detectors for the detection of shocks and a classification of them into four types. Second, we show that shock patterns are not arbitrary, but obey the rules of a grammar which limits the possible shock combinations. In addition, shock patterns satisfy specific topological and geometric constraints. We develop this shock grammar and exploit the topological and geometric constraints to enforce *global* consistency: shock hypotheses that violate the grammar or are topologically or geometrically invalid are pruned, and survivors are organized into higher level structures. The result is a computational method for the detection, classification, and grouping of shocks. This leads to a description of shape as a hierarchical graph of shock groups. The graph is computed in the reaction-diffusion space, where diffusion plays a role of regularization to determine the significance of each shock-group. The representation is stable with rotations, scale changes, occlusion, movement of parts, noise and other variations, even at very low resolutions. We illustrate the suitability of this representation for recognition by discussing several examples.

Keywords: *recognition, shape representation, shock detection, shock grammar, multi-scale representation, skeletons, curve evolution.*

Figure 1: Can you recognize these birds? Whereas a name for each bird eludes the naive observer, they are effortlessly grouped into two categories, based on similarity in "form".

1 Introduction

What does it mean to *recognize* an object from its shape? Informally, this implies an identification of the shape with a familiar category or class of objects. Clearly, this association can be made at several different levels: at one level the silhouettes in Figure 1 are identified as belonging to the category "bird", at another they are divided two sub-categories, based on similarity in form[1]. This notion of categorization is crucial to many vision tasks, such as searching a database of shapes rapidly, reasoning about the attributes of new or unfamiliar shapes, *etc.* Curiously, whereas this ability to categorize appears to come naturally and effortlessly to humans, it has been extremely difficult to formalize for computers. In this paper, we address the computational aspects of this problem; specifically, we investigate the description of generic shape classes from the mathematical perspective of curve evolution.

Existing proposals for shape representation are often classified according to those that are region-based, emphasising properties such as symmetry and thickness, versus those that are boundary-based, emphasising salient features of the shape's boundary such as curvature extrema and inflection points. Prominent examples of region-based representations include Blum's *symmetric axis transform* (SAT) [4, 5], motivated by the need for a geometry that captures biological shape and describes its growth, and the related *smoothed local symmetries* (SLS) [7] and *process inferring symmetric axis* [38]. Well studied examples of boundary-based descriptions include polygonal approximations of a shape's contour, and Hoffman and Richard's representation based on *codons*, or contour segments bounded by minima of curvature, the latter motivated by a transversality-based proposal for parts [22]. However, it is important to note that these classifications are not mutually exclusive, nor are they unique. First, it may in fact be desirable to capture both boundary as well as region-based features, as is the case in Pizer *et al.*'s *core* based model, where the scale at which boundaries are detected and described is a function of the width of the object through its region [10]. Second, an orthogonal classification is that

[1]The avid bird-watcher will assign these the labels "hawk" and "cormorant".

of primitive-based approaches, where shape is viewed statically as a combination of a small number of components, *e.g.*, *generalized cylinders* [42], or *geons* [3] , versus process-based approaches [38] where shape is explained dynamically or developmentally via a set of processes acting on a simpler shape.

Returning to Blum's proposal of a sphere as a primitive basis for modelling object growth, this view has spawned a vast literature on the theoretical and computational aspects of skeletons. However, it is unfortunate that Blum's key insight that the SAT provides for qualitative shape descriptions in terms of "shape morphemes", *e.g.*, disc, worm, wedge, flare, *etc.* [5, 6], is usually forgotten. More specifically, Blum points out that the *grassfire* formulation, where the symmetric axis is obtained as quench points of a grassfire moving parallel to the boundary, places an ordering on the locus of skeletal points defined by the direction of grassfire flow (the direction of increasing object width). This allows for a number of qualitative shape properties to be extracted via the axis curvature, the velocity along the axis (object angle) and its discontinuities, *etc.* Curiously, an evolutionary approach to shape description supports and complements this view, and gives it a sound mathematical foundation [28, 29, 31]. To elaborate, Kimia *et al.* suggest a representation based on deformations of the shape's boundary:

$$\begin{cases} \frac{\partial \mathcal{C}}{\partial t} & = \beta(.)\vec{N} \\ \mathcal{C}(s,0) & = \mathcal{C}_0(s), \end{cases} \tag{1}$$

where $\mathcal{C}$ is the boundary vector of coordinates, $\vec{N}$ is the outward normal, s is the path parameter, t is the time duration (magnitude) of the deformation, and β is arbitrary. A special case is when the deformation is a linear function of curvature $\beta(.) = \beta_0 - \beta_1\kappa$, leading to:

$$\boxed{\begin{cases} \frac{\partial \mathcal{C}}{\partial t} & = (\beta_0 - \beta_1\kappa)\vec{N} \\ \mathcal{C}(s,0) & = \mathcal{C}_0(s). \end{cases}} \tag{2}$$

The space of all possible deformations in this form is spanned by two parameters: the ratio of the coefficients β_0/β_1 and time, t, constituting the two axes of the *reaction-diffusion space*. Underlying the representation of shape in this space are a set of *shocks* [34], or entropy-satisfying singularities, which develop during the evolution. These are points where some information is lost during the deformation process, such as discontinuities in orientation along the boundary of the shape, or the collision of remote portions of the shape through its interior. The connection between shocks and skeletons is that the reaction axis corresponds to a grassfire simulation. Thus, the set of shocks which form along the reaction axis, $\beta_1 = 0$, is indeed Blum's skeleton [4] [2], see Appendix A. Shocks form along other axes of the reaction-diffusion space as well, and are classified into four types [28, 31], (Figure 2):

Definition 1 *A* FIRST-ORDER SHOCK *is a discontinuity in orientation of the boundary of a shape.*

[2] In his grassfire formulation Blum called these *generalized corners* [5].

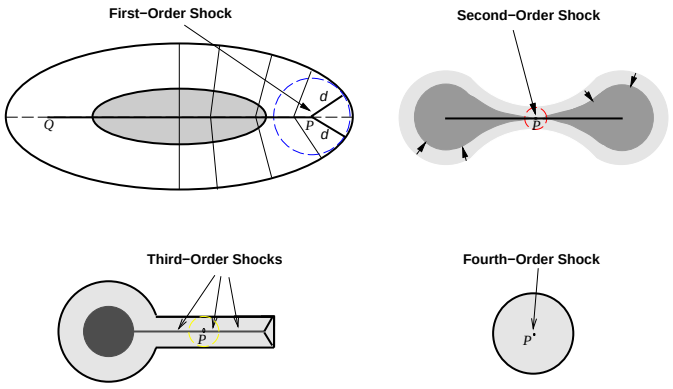

Figure 2: This figure depicts the four types of shocks formed in the course of the deformation process; each is correlated with a perceptual/semantic category, *i.e.*, *protrusion*, *part*, *bend* and *seed*. For each shock type, the maximal inscribed disc is overlayed.

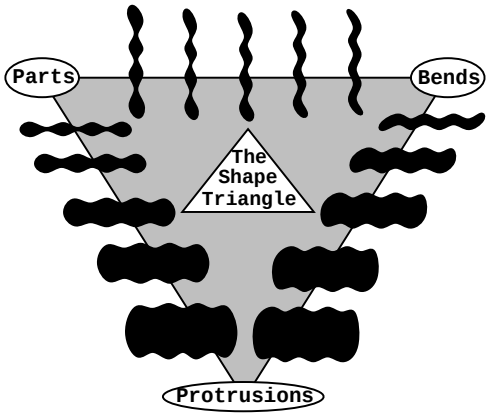

Figure 3: The nodes of the *shape triangle* represent three cooperative/competitive processes acting on shape, namely, parts, protrusions, and bends. The sides of the triangle represent continua of shapes whose extremes correspond to each node [30].

Definition 2 *A* SECOND-ORDER SHOCK *is formed when two distinct non-neighboring boundary points join, but none of their immediate neighbors collapse together.*

Definition 3 *A* THIRD-ORDER SHOCK *is formed when two distinct non-neighboring boundary points join, such that the neighboring boundary points also collapse together.*

Definition 4 *A* FOURTH-ORDER SHOCK *is formed when a closed boundary collapses to a single point.*

A key aspect of shocks is that they allow for precise *quantitative* descriptions of shape, on the one hand, and more *qualitative* perceptual ones, on the other. Specifically, each shock-type is correlated with an intuitive perceptual property of the shape, Figure 2: 1) a first-order shock is formed from a *protrusion* on the shape's boundary, 2) a second-order shock signals the splitting of the shape into two parts at a *neck*, 3) a collection of third-order shocks may be interpreted as a *bend* [3], and lastly 4) viewing the evolution in reverse, a fourth-order shock is a *seed* from which the shape is born. The grouping and organization of shocks into these higher level data structures provides the basis for the categorical theory of shape we adopt. The psychophysical relevance of this model is investigated in [30], where the cooperation and interaction between the *parts*, *protrusions*, and *bends* processes is reflected by three separate continua, Figure 3.

While the above definitions of shock types are intuitive, they do not easily lend themselves to algorithms for shock detection. The focus of the current paper is twofold: (i) on the computational aspects

[3] Whereas in the strict sense third-order shocks are not generic, they are important enough to merit a distinct classification for several reasons, see Section 5.

of deriving a representation based on singularities formed in the course of shape evolution, namely, the numerical detection and classification of shocks, and (ii) on the dynamic organization of shocks in the form of groupings into higher level data structures via a shock grammar. The detection of shocks on a discrete grid is an inherently difficult problem: it is not clear how to distinguish between singularities that are artifacts of discretization, and those that are locally "weak", but structurally valid. The situation is reminiscent of the dilemma between weak edges and false positives in edge detection. An approach that has proven to be successful in that domain is one of dividing the task into two stages: 1) a local detection stage giving rise to true as well as some spurious edges [23], and 2) a global interpretation stage which strengthens edges with lateral support through a relaxation process [60, 49]. Similarly, a key idea of this paper is that shock computations can be made robust by relying not only on better (subpixel) *local* detectors and classifiers, but also on the *global* interactions among them through a shock grammar. The shock grammar allows us to rule out impossible shock combinations, as well to group shocks into connected components, leading to a hierarchical representation that can be functionally related to the shape's parts, protrusions, and bends.

In related work, Leymarie and Levine have simulated the grassfire transform using active contours moving so as to seek minimum potential energy configurations on an inverted distance surface [36], an approach which enables the use of a Euclidean metric while bypassing discretization problems in typical skeletonization algorithms. Further, a notion of "branch significance" is introduced, based on measuring the amount of local deformation on the distance surface induced by a particular branch. In effect, this is an approximation of the propagation velocity of a shock, a criterion for significance proposed by Blum [4]. Scott *et al.* have suggested the use of wave propagation to obtain the full symmetry set, *i.e.*, the locus of centers of *all* bi-tangent circles whether or not they are contained within the shape [54]. Theirs is an alternating scheme of propagating waves from edge-points in a binary image, and damping them via the diffusion or heat equation. By superposition, the maximum energy to arrive at a location, along with its arrival time gives the radius of the strongest symmetry axis about that point. In effect this is equivalent to measuring the radial symmetry about a point by convolving the edge map with an annulus whose width is proportional to its inner radius. Kelly and Levine have demonstrated the use of annular operators in obtaining coarse object descriptions from real imagery, containing textures, gaps, internal structures, and contrast-sign reversals along occluding contours [25]. Annular operators at increasing scales are applied to edge maps obtained at corresponding scales, to extract a set of symmetry points at each scale. The symmetry points are grouped into types of parts: "limbs" and "blobs". Motivated by psychophysical and physiological evidence, Pizer *et al.* have proposed a computational model for object representation via "cores", or regions of high medialness in intensity images [51, 10]. In this model, boundary detectors operate over a range of scales, but connections are only made between detectors operating at the same scale, and at spatial distances proportional to the scale in question. Thus, the core model shares an important

property with Scott *et al.*'s and Kelly and Levine's proposals: the scale at which boundary detail is represented depends upon the object width in that region.

Our approach extends the above work in a number of ways. First, unlike these approaches, ours provides a classification of skeletal points according to shock types, leading to generic perceptual shape classes with semantic meaning (parts, protrusions, bends, seeds). Second, our approach does not require any sort of preprocessing, such as finding positive maxima in order to initialize snakes [36], or to segment the boundary [32], and can deal with arbitrarily complex shapes exhibiting numerous topological splits as the front evolves. Third, to our knowledge, the explicit use of a shock grammar to prune impossible shock configurations is new. Finally, following the theoretical ideas in [28], the computational use of curvature deformation (β_1) to assign a significance to each shock group is novel.

The paper is outlined as follows. In Section 2, we develop local operators for detecting shocks as well as for classifying them into four types with subpixel accuracy. In Section 3, we develop a grammar for shock formation, and design an algorithm for enforcing consistency between shock hypotheses: impossible shock combinations are pruned and survivors are dynamically organized into shock groups. We illustrate our algorithms on a variety of computational examples in Section 4. In section 5 we explore the role of diffusion as a regularizing element to each shock group, leading to a notion of "structural diffusion". This is a key step in building a hierarchical model of shape for recognition and allows a sorting of shape information into a sequence from quantitative to qualitative. Finally, whereas we have assumed the availability of a segmented shape as an initial step, in Section 6 we suggest how the shock-based framework might be extended to apply directly to images.

2 Shock Classification and Detection: Local Operators

Whereas at first glance shock detection might appear to be a straightforward task (*e.g.*, corner detection algorithms [13, 59] can be used to locate first-order shocks), finding singularities, particularly in low resolution cases, remains a challenging problem. The first difficulty is to arrive at a complete classification of shocks that leads to a computational algorithm for detecting them. The approach proposed here classifies shocks based on the properties of a surface in which the evolving shape is embedded as a level set. The second difficulty is to obtain accurate geometric estimates for shock detection without blurring across singularities. Our approach utilizes the high resolution information present in the embedding surface. We employ a smoothing algorithm that provides reliable geometric estimates while leaving singularities intact, resulting in subpixel shock localization. We now discuss shock classification and detection in turn.

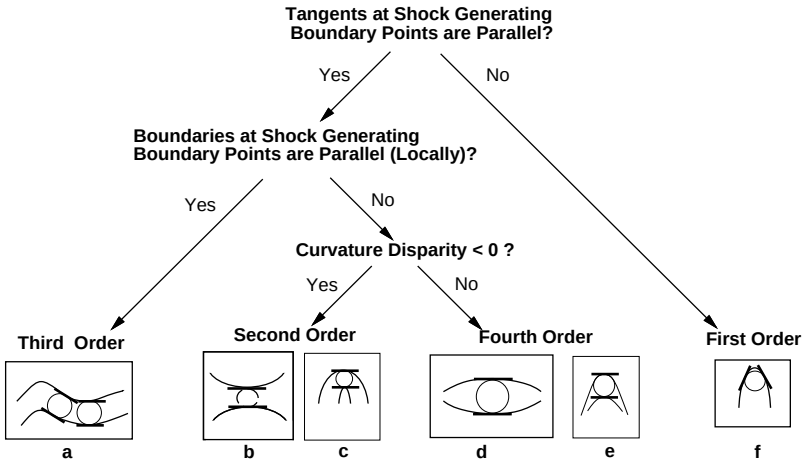

Figure 4: A classification of shock types based on the tangents of the boundary points that form the shock, the curvature at those points, and on their local neighborhood.

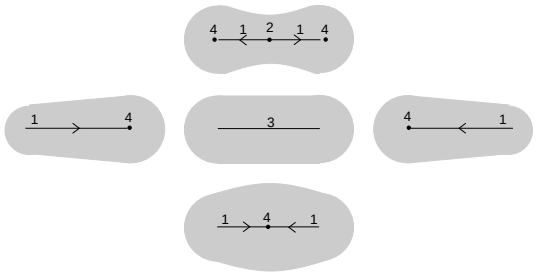

Figure 5: Third-order shocks provide a categorical reference for fast moving first-order shocks, travelling in opposite directions.

2.1 Classification of Shocks

While the definition of shocks in the introduction is motivated by events in the dynamic evolution of a shape, it does not immediately lead to a computational algorithm for the classification of shocks. An intuitive approach is to rely on properties of the boundary points which collide at the shock, as illustrated in Figure 4. If the associated bi-tangents are not parallel, it must be a first-order shock, travelling in the direction of increasing object width. If the tangents are parallel the shock type depends on the local neighborhood of the shock generating boundary points. If the boundaries are parallel (locally), they will remain parallel in the course of the evolution, thus colliding at a set of *third-order shocks*. If not, the shock-type depends on the curvature disparity, *i.e.*, the sum of the signed curvatures at each shock generating boundary point. If this quantity is negative, we have a local minimum in shape width and hence a second-order shock. On the other hand, if it is positive we have a local maximum in shape width and hence a fourth-order shock.

Whereas third-order shocks are not generic (two boundaries have to be exactly parallel in order for them to form), they are important enough to merit a distinct classification for several reasons. First, third-order shocks represent a type of symmetry that is abundant in a large variety of biological as well as man-made objects which have "bend-like" components, *e.g.*, consider the fingers of a hand, limbs of animals, branches of a tree, the legs of a table or a chair, the handles of a pair of pliers, the blade of a screw-driver, *etc.* Second, third-order shocks are simultaneously the limit of two distinct groups: first-order shocks travelling with infinite speed, but in opposite directions, Figure 5. They serve as a categorical reference for such groups, in the same way that vertical objects are referred to slightly tilted ones in human perception [39]. Third, when sampled on a discrete grid a pair of continuous space parallel curves shares a digital representation with a pair of "almost" parallel curves. Hence, the set of parallel curves on a discrete grid is no longer negligible. Finally, the psychophysical results

of [30] suggest that along the parts-bends and protrusion-bends continua, Figure 3, there are transition points beyond which subjects place shapes at the "bends" node despite the fact that their boundaries are not exactly parallel.

Whereas the classification of Figure 4 provides insight, it is difficult to implement directly. Consider, for example, the potential bookkeeping problems in mapping shock points to their associated bi-tangents, particularly in the presence of multiple nearby topological splits, as occur at third-order shocks. Alternatively, one may rely on the differential properties of the *embedding surface*, which proves to be computationally efficient and robust. To motivate the need for an embedding surface, recall that it is not clear how to evolve the curve by equation (2) once singularities have formed, since the differential notions of normal, curvature, *etc.*, are no longer defined. As a remedy to this problem, classical differential geometric notions are considered in the *generalized* or *weak* sense by using the concepts of entropy [34] and viscosity solutions [41, 12, 11]. For theoretical as well as numerical reasons, the original curve flow is embedded in the level set evolution of an evolving surface [15, 48, 2], $z = \phi(x, y, t)$, with the correspondence that the evolving shape is represented at all times by its zero level set $\phi(x, y, t) = 0$. It can be shown that the zero level set of surfaces evolving according to

$$\phi_t + \beta(\kappa)|\nabla\phi| = 0 \tag{3}$$

correspond to the viscosity solutions of (1) [2]. The numerical simulation of (3) was first proposed by Osher and Sethian [56, 48] who provided an elegant scheme for flame front propagation. We utilize this scheme for shape evolution; for convenience we take ϕ_0 to be the distance transform of the shape. We now describe a classification of shocks based on the differential properties of the embedding surface ϕ, Figure 6.

A **first-order** shock can be detected as a discontinuity in the orientation of the tangent $\vec{T}$ to the curve $\mathcal{C}$; which may computed from ϕ as $\arctan(\frac{-\partial\phi/\partial x}{\partial\phi/\partial y})$. The embedding surface has a discontinuity as well, Figure 6 (top left). On a discrete lattice, a discontinuity in orientation is locally indistinguishable from a curvature extrema with sufficiently high curvature. Thus, a first-order shock may be detected as a local maximum in orientation change between neighboring boundary points, where this orientation change exceeds a threshold[4].

At a **second-order** shock the shape undergoes a topological split at an isolated point; here the embedding surface must be hyperbolic, Figure 6 (top right). This follows from the fact that the initial distance transform surface is monotonically non-decreasing (as one moves inwards from the zero-level set), and that it remains monotonically non-decreasing in the course of evolution by (3), where $\beta(\kappa) = \beta_0 - \beta_1\kappa$. In the vicinity of the "neck", the surface is *hyperbolic*: it rises in one principal

[4]In Section 2.2 we revise this computation to better distinguish between high curvature points and discontinuities, by using subpixel interpolation methods.

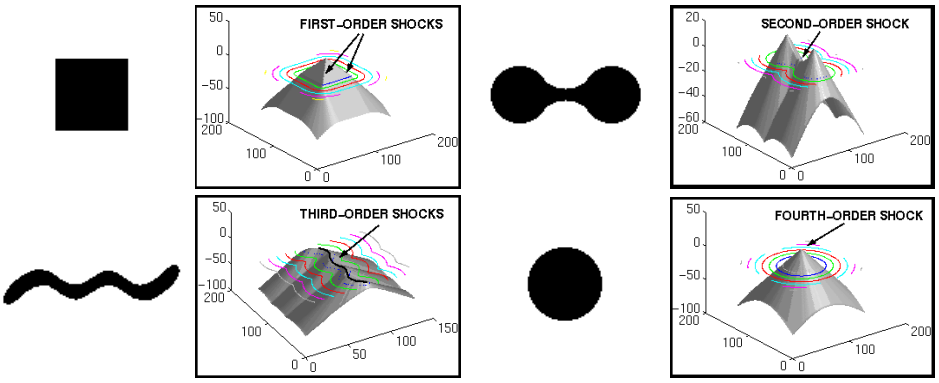

Figure 6: A classification of shock types based on properties of the embedding surface (in this case the distance transform ϕ), shown on the right of each shape. Top Left: First-order shocks occur at corners of the square shape, corresponding to creases on the surface with $|\nabla\phi| > 0$. Top Right: A second-order shock forms at the "neck" of the peanut shape, corresponding to a hyperbolic point with $|\nabla\phi| = 0$. Bottom Left: A set of third-order shocks forms along the central axis of the worm shape, where $\kappa_1\kappa_2 = |\nabla\phi| = 0$. Bottom Right: A fourth-order shock forms in the center of the circle shape, where $\kappa_1\kappa_2 > 0$ and $|\nabla\phi| = 0$.

Shock Type	Orientation	Curvature
First-Order	non-vanishing $\nabla\phi$	high level set curvature
Second-Order	isolated vanishing $\nabla\phi$	$\kappa_1\kappa_2 < 0$
Third-Order	non-isolated vanishing $\nabla\phi$	$\kappa_1\kappa_2 = 0$
Fourth-Order	isolated vanishing $\nabla\phi$	$\kappa_1\kappa_2 > 0$

Table 1: This table depicts the classification of shock types based on the gradient, the level set curvature, and the principal curvatures of the surface.

curvature direction and falls in the other. Further, since the colliding boundary points have normals pointing in opposite directions, $|\nabla\phi|$ must go to zero at the point of collision. Thus, second-order shocks are detected as hyperbolic points where the gradient of the surface approaches zero.

Next, **third-order shocks** are formed when an entire boundary segment collides with another. At these points the corresponding surface ϕ is *parabolic*, Figure 6 (bottom left), and since pairs of colliding boundary points have normals pointing in opposite directions, once again $|\nabla\phi|$ must go to zero.

Finally, **fourth-order shocks** are formed when an entire closed boundary collapses into a single point. At these points, the corresponding surface ϕ attains a local maximum in height, Figure 6 (bottom right). Therefore, the surface is *elliptic* (the principle curvatures κ_1, κ_2 are positive), and once again, $|\nabla\phi| = 0$.

Table 1 summarizes the classification of shocks based on differential properties of the embedding surface [5]. Note that shocks are properties of the zero level set, whose evolution is invariant to the choice of the

[5]It should be noted that all the necessary quantities can be computed from a local neighborhood of ϕ:

initial embedding surface ϕ_0, so long as it is Lipshitz continuous [15, 11]. The classification of shocks is therefore also invariant to the choice of embedding surface, provided it is monotone in moving from one level set to the next. This classification provides a theoretical grounding for our shock detection algorithm, as discussed in the following section.

2.2 Subpixel Shock Detection

Shocks occur as discrete events in time and space; it is easy to miss them if computations are isolated to grid points, without exploiting the continuous propagation of information that is implicit in curve evolution. We therefore develop a subpixel implementation of the above ideas, motivated by two observations. First, standard techniques such as central differences blur across discontinuities (where typically the shocks lie) and provide unreliable estimates of geometric quantities, *e.g.*, orientation, in their vicinity. Accurate estimates of orientation are important not only for shock detection, but also for estimating shock velocity, Appendix B, used to group shocks. Second, "true" shocks typically lie *between* grid points. Whereas the level set formulation (equation 3) supports subpixel curve evolution, an algorithm that only attempts to locate shocks at grid points will suffer from discretization artifacts and will not provide smooth shock paths.

To address the problem of inaccurate differential estimates in the vicinity of discontinuities, a class of schemes have recently been proposed in the numerical analysis literature, in application to the numerical solution of conservation laws and the propagation of fronts. These *essentially non-oscillatory* (ENO) schemes were introduced by Harten *et al.* [20], and were later made more efficient by Shu and Osher [57]. The basic idea is to select between two contiguous sets of data points for interpolation the one which gives the lower variation, or coefficient of the highest derivative of an interpolation polynomial. At regions neighboring discontinuities, the smoothing is always from the side *not* containing the discontinuity. Siddiqi *et al.* have adapted these ideas to the 2D problem of locating level curves of an embedding surface while: 1) not blurring across discontinuities, and 2) explicitly and accurately placing them [58]. The key idea is to replace polynomials with *geometric* interpolants: lines, circular arcs, Euler spirals, *etc.*, while also allowing for "breaks" in the interpolated curve[6]. This *geometric essentially non-oscillatory* (GENO) approach provides a subpixel contour tracer that can be used to find high resolution level curves (open or closed) of an intensity surface, without explicitly constructing or representing a subpixel surface. We utilize this algorithm to obtain the shape's contour from the embedding surface, with important advantages for shock detection. In particular, *corners* or first-order shocks, are explicitly placed, and multiple curve segments per pixel (such as when two

$|\nabla\phi| = (\phi_x^2 + \phi_y^2)^{1/2}$; $\kappa_1\kappa_2 = \frac{\phi_{xx}\phi_{yy} - \phi_{xy}^2}{(1+\phi_x^2+\phi_y^2)^2}$; $\kappa_1 + \kappa_2 = \frac{(1+\phi_x^2)\phi_{yy} - 2\phi_x\phi_y\phi_{xy} + (1+\phi_y^2)\phi_{xx}}{(1+\phi_x^2+\phi_y^2)^{3/2}}$.

[6] This is in essence Harten's "sub-cell resolution" idea [19], the difference being that geometric reasoning is used in place of conservation to determine the sub-cell shock location.

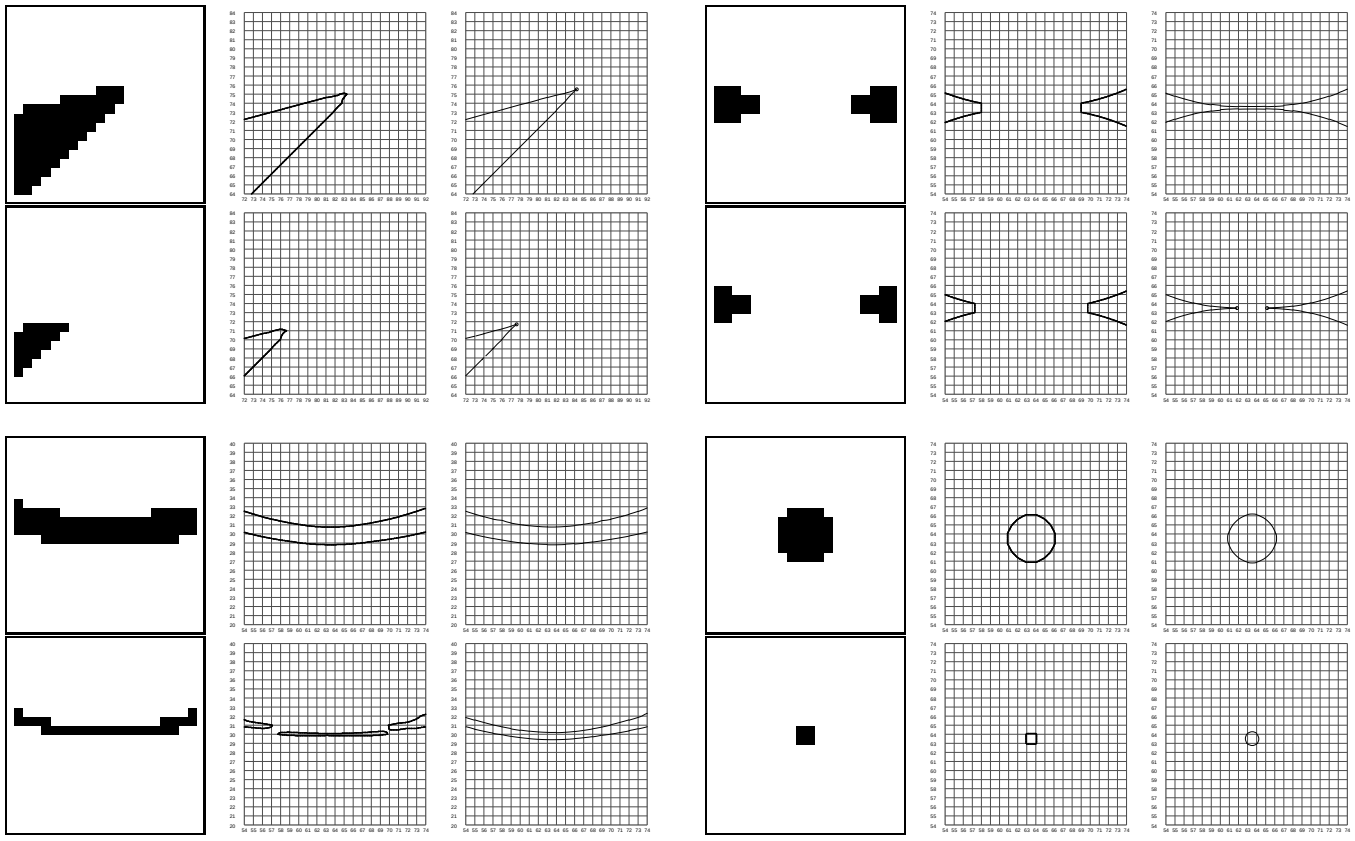

Figure 7: A comparison of interpolation techniques. Each row depicts the interior of the shape at the resolution of the grid (left), the bilinear interpolation of the boundary (middle) and the *geometric ENO* (GENO) interpolation of the boundary, with detected corners marked with circles (right). Whereas discretization results in a "jagged" appearance, GENO and bilinear interpolation are comparable in smooth regions. However, in contrast to bilinear interpolation, GENO is able to: i) capture the corner of the evolving triangle with subpixel resolution and without introducing artifacts (first-order shock, TOP LEFT), ii) detect and represent the topological split at the neck, followed by the formation of cusps on either side (second-order shock, TOP RIGHT), iii) represent the collapse of the bend without introducing artifacts (third-order shock, BOTTOM LEFT), and iv) preserve the "circular" shape of the circle even when it becomes very small (fourth-order shock, BOTTOM RIGHT).

opposing boundary segments are about to collide) can be represented, Figure 7. However, the algorithm does not directly provide higher-order shocks. In order to use it for second-, third-, and fourth-order shock detection, a further development is necessary, discussed in the following.

Recall that all higher-order shocks share the property that the gradient of the embedding surface must go to zero, Table 1. Hence an obvious approach to shock detection is to locate zeros of $|\nabla\phi|$ and then classify them as one of three shock types, based on the Gaussian curvature of ϕ. However, the first step, that of locating zeros of $|\nabla\phi|$, is not as straightforward as it may appear. Observe that the magnitude of the gradient typically goes to zero *between* and not at grid points. In fact, at grid points in the vicinity of a potential zero the gradient may already have an appreciable magnitude. A strategy of flagging grid points where $|\nabla\phi|$ falls below a chosen ϵ cannot escape the trade off between achieving

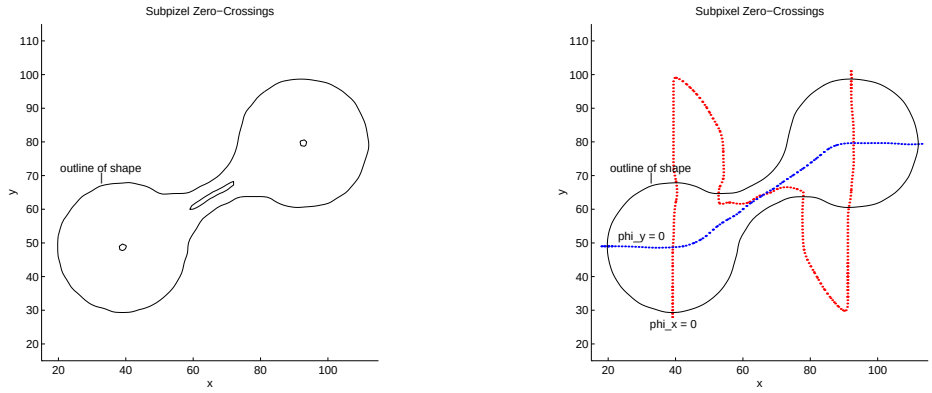

Figure 8: Subpixel detection of higher order shocks for a peanut shape. LEFT: The zero-crossing contours of $(|\nabla\phi| - \epsilon)$ demarcate regions around the putative shock points. RIGHT: Zero-crossings of ϕ_x and ϕ_y. Observe that the level curves intersect at *exactly* three points. Two of these are fourth-order shocks, and the middle one is a second-order shock, as can be determined from the sign of ϕ's Gaussian curvature.

good localization (for which $\epsilon \to 0$) and reducing the probability of missed shocks (for which ϵ has to be large). One way to combat errors due to discretization is to utilize the subpixel contour tracer to find ϵ crossings of $|\nabla\phi|$, as illustrated for the peanut shape in Figure 8 (left). Nevertheless, such an approximation will always yield 2D *regions* surrounding the putative shock points, and not the actual shock locations themselves.

As a solution to this dilemma, we make the observation that in order for $|\nabla\phi|$ to go to zero, ϕ_x *and* ϕ_y *must each go to zero independently.* In other words, we can effectively reduce a 2D problem to two 1D problems, by considering zero-crossings of ϕ_x and ϕ_y. Whereas the two approaches are theoretically equivalent, numerical approximations of the latter reduce one dimension of ambiguity. To illustrate, observe that for the peanut shape, approximations of $|\nabla\phi| = 0$ yield 2D regions, Figure 8 (left), while independent approximations of $\phi_x = 0$ and $\phi_y = 0$ as two 1D curves admit the use of the GENO subpixel tracer, Figure 8 (right). Note that while $|\nabla\phi|$ is nonnegative and never actually crosses zero, ϕ_x and ϕ_y do cross zero. At locations where $\phi_x = 0$ and $\phi_y = 0$ simultaneously, we have shock points, Figure 8 (right). Two of these are fourth-order shocks, and the middle one is a second-order shock, as can be determined from the sign of the Gaussian curvature of the surface ϕ. This leads to the following algorithm for obtaining subpixel second-, third-, and fourth-order shocks:

1. Construct the surfaces ϕ_x, ϕ_y. For each surface, utilize the subpixel contour tracer to obtain all zero-crossing curves (open as well as closed), each curve being an ordered set of (x, y) data points[7].

[7]Note that an exception occurs when either ϕ_x or ϕ_y is identically zero over a neighborhood of grid points. This can happen, for example, when the original shape has a straight edge parallel to one of the coordinate axes. In such a case, the initial embedding surface ϕ_0, obtained as the signed distance function of the shape, is constant in the direction of that axis, in the vicinity of the edge. Therefore, such regions must be marked prior to interpolating level curves. Fortunately, the monotone condition on ϕ implies that ϕ_x and ϕ_y cannot both be identically zero over the same regions, since that would imply a 2D region of third-order shocks, which is an impossibility.

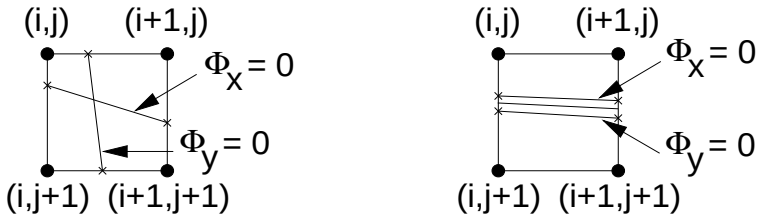

Figure 9: The detection of second-, third-, and fourth-order shocks, based on overlaps of $\phi_x = 0$ and $\phi_y = 0$ within a cell. The four neighboring grid points are marked with filled circles. LEFT: When the two curves pass through the same cell and are not parallel, a second-order or fourth-order shock is placed at the point of intersection (provided that it lies within the cell), based on the sign of the Gaussian curvature. RIGHT: When the two curves pass through the same cell and are close to parallel, a set of third-order shocks is interpolated as a line drawn through the averaged endpoints.

Store the two collections of curves in the sets S_x and S_y respectively.

2. For each curve $C_i \in S_x$ examine each curve $C_j \in S_y$ for overlaps, as illustrated in Figure 9. Specifically, for a given curve, each successive pair of data points define the entry and exit points in a cell. Two curves C_i and C_j can overlap when they pass through the same cell, and either intersect or are very close. The nature of the overlap can be analyzed by examining the slopes of the line segments connecting the entry and exit points. When the two segments are not parallel, either a second-order or a fourth-order shock is placed at the intersection point, as determined by the sign of the Gaussian curvature, Figure 9 (left). On the other hand, if they are parallel, *i.e.*, level curves overlap over a neighborhood, a set of third-order shocks is placed, since they are the only possible non-isolated higher-order shocks, Figure 9 (right)[8].

3. Finally, form third-order shock groups by following the points on each C_i and C_j, and linking third-order shocks in neighboring cells.

In the following section we examine three types of constraints on shock patterns, leading to rules for pruning shock hypotheses and organizing survivors into groups, consistent with the global history of shocks.

3 Shock Grouping: Global Interactions

Blum's grassfire formulation provides a definition for the skeleton of a shape as the set of *generalized corners* that form as the grassfire propagates [4]. Indeed, it can be formally shown that the set of shocks and their formation times under pure reaction ($\beta_1 = 0$), provides the set of skeletal points, and its associated radius function, Appendix A. This implies that geometric and topological properties that hold for skeletons, studied by Giblin *et al.* [17, 9, 8], Matheron [43], Meyer [44], among others,

[8]In our implementation the two segments are considered parallel when their slopes are within 10 degrees. In this case a set of third-order shocks is interpolated as a line between the averaged endpoints.

must hold for shocks as well, *i.e.*, shocks depend on neighboring (in space and time) shock patterns. In Section 3.1 we examine three types of constraints on shock formation: *sequential, geometric* and *topological*. Sequential constraints pertain to the composition of a shock group (an allowed sequence of shocks) and are concisely described using a grammar for shocks; geometric and topological constraints relate to properties of one or more shock groups (smoothness, connectivity, *etc*). In Section 3.2 we exploit these constraints to prune shocks detected by our subpixel algorithm (Section 2) that violate the rules of formation, such as isolated first-order shocks, and to organize the survivors via more global structures, *e.g.*, "protrusions" and "bends".

3.1 A Grammar for Shocks

The fact that not all shock patterns are possible provides powerful constraints for pruning shocks that are locally detected, but are globally inconsistent. This leads to more robust shock computation. For example, consider a first-order shock path terminating in a point which is detected as a potential second-order shock. This pattern is not possible, and therefore the second-order shock should be pruned. In the following we examine sequential, geometric and topological constraints on shock formation, and summarize the sequential constraints via a concise grammar for shocks. We begin by defining initial and terminal shocks:

Definition 5 *An* initial *shock is one which may subsequently give rise to other shocks, but can have no shocks flowing into it.*

Definition 6 *A* terminal *shock is one which has no shocks flowing out of it, but may have shocks flowing into it.*

Proposition 1 *First order shocks flow with finite speed, except for a set of isolated points* (e.g., *initial first-order shocks flowing outwards from a second-order shock).*

Proof: Suppose that on the contrary, there exists a path of infinite velocity first-order shocks. Then, from Appendix B, we have the relation $s = \frac{\beta_0}{sin(\theta/2)}$, where s is the first-order shock velocity, β_0 is the speed at which the front is propagating, and θ is the angle between the colliding boundary tangents at each shock. An infinite velocity path implies that $\theta = 0$, *i.e.*, the boundary tangents are parallel throughout, and therefore we have a path of third-order shocks. On the other hand, isolated infinite velocity first-order shocks are possible, *e.g.*, the initial first-order shocks to flow outwards from a second-order shock, as will be explained shortly.

Proposition 2 *Third-order shock directions change continuously,* i.e., *a third-order shock branch cannot have any corners.*

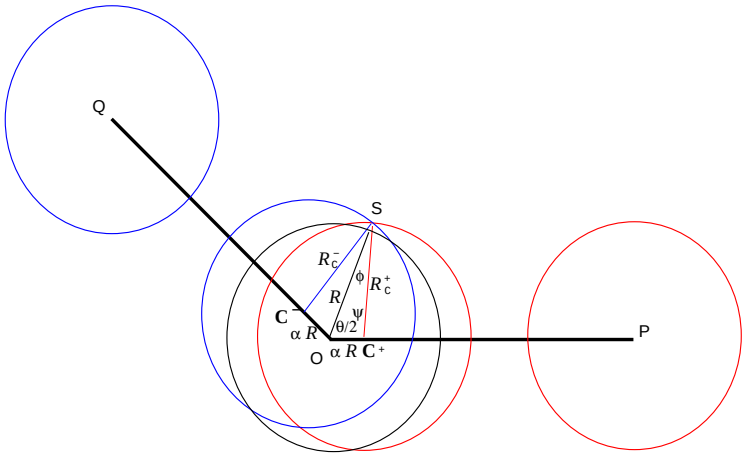

Figure 10: First-order and third-order shock-branches cannot have a corner.

Proof: Assume that there exists a third-order shock path with a discontinuity at point O, Figure 10. We will show that this leads to a contradiction. Let OP and OQ denote the tangents to the shock path at either side of the discontinuity O, forming an angle $\theta < \pi$. Since O is itself a shock, there exists a maximal circle of radius R that is at least bi-tangent to the shape. Consider two points C^+ and C^-, one on each side of the discontinuity, and circles of radius R_C+, and R_C-, at each point respectively. Let S denote the point of intersection of the circles on the convex side of the discontinuity. First consider a third-order shock path, such that $R_C+ = R_C- = R$. Let $OC^+ = OC^- = \alpha R$. Observe that ϕ can be made small by picking a small α, such that $\lim_{\alpha\to 0}\phi = 0$. Similarly, from triangle OSC^+, $\psi = \pi - \frac{\theta}{2} - \phi$ so that $\lim_{\alpha\to 0}\psi = \pi - \frac{\theta}{2}$. Since $\theta < \pi$ and $\psi > \frac{\pi}{2}$ in a sufficiently small neighborhood of O, $\psi > \frac{\theta}{2}$ in the triangle OSC^+, implying that $OS > R_C+ = R$. This violates the property that the circle of radius R centered at O is maximal, contradicting our initial assumption. A similar argument holds for first-order shock paths (neglecting their endpoints, which can of course branch).

Proposition 3 *First-order shock directions change continuously,* i.e.*, a first-order shock branch cannot have any corners.*

Proof: The proof is similar to that of Proposition 2, with the modification that we can no longer assume $R_C^- = R_C^+ = R$. In fact, with the shock at C^- occurring first, it is now the case that $R_C^- < R < R_C^+$. However, we can still show that $OS > R$, violating the assumption that the circle of radius R centered at O is maximal, *i.e.*, that O is a skeletal point. Note that by Proposition 1, first-order shock velocities are finite and can therefore be bound in a small neighborhood of point O. As such, the times of formation of C_- and C_+, R_C+ and R_C- respectively, can be made arbitrarily close to one another, since $\lim_{\alpha\to 0}\phi = 0$. Thus, a similar argument applies as that for Proposition 2, implying that $OS > R_C+ > R > R_C-$.

Proposition 4 *Second-order shocks are initial. No shocks can flow into them, and they are isolated from other second-order, third-order, and fourth-order shocks.*

Proof: The fact that a second-order shock is isolated from other second-, third-, and fourth-order shocks follows from its definition. It remains to be shown that a discontinuity in orientation (a first-order shock) does not occur at one or both of the boundaries exactly at the point of second-order shock formation. In other words, we must show that the tangent to each of the colliding boundaries exists at the second-order shock. This property holds due to the following theorem, proved in [26]:

Theorem 1 *When two distinct non-neighboring points of the boundary come together, the tangents at these points exist, and are parallel.*

Remark 1 *Once formed, a second-order shock must give rise to two first-order shocks that flow out of it. The speed of each first-order shock is infinite.*

Explanation: By Theorem 1, at the second-order shock the boundary tangents are parallel. Hence, following the split, there is a discontinuity in orientation of π radians on either side, giving rise to two first-order shocks. Since the angle between the colliding tangents is zero on either side of the second-order shock, the first-order shock speed, given by $s = \frac{\beta_0}{sin(\theta/2)}$, is infinite. Further, since the curvature disparity must be negative for a second-order shock to form, the resulting first-order shocks must flow away from the second-order shock (in the direction of increasing shape width).

Proposition 5 *A first-order shock branch can either merge with another first-order shock branch, terminate in a third-order shock branch, or terminate in a fourth-order shock.*

Proof: A first-order shock branch cannot simply terminate, since characteristics push into a shock and hence, in the absence of interference from other shocks, a discontinuity in orientation travels as one[9]. Further, it cannot terminate in a second-order shock by Proposition 4. Therefore, the only possibilities are those listed above.

Proposition 6 *Two third-order shock branches cannot intersect.*

Proof: Let S_1 be a third-order shock branch, with an associated time of formation T for each shock in it, Figure 11. Consider the area formed by the union of all circular disks of radius $\beta_0 T$, one centred at each shock. By Hüygens' Principle and the entropy condition, a point is contained in the shape, if it lies in any such disk, otherwise it must lie outside the shape. Now let S_2 be a curve which intersects S_1 at X. Consider a point P on S_2, and let d be the distance from P to S_1. Note that if P is third-order shock with time of formation $\mathcal{T}$, a disk of radius $\beta_0 \mathcal{T}$ must be entirely contained within the shape. From Figure 11 we see that this contradicts the requirement (for S_1 to be a third-order shock branch) that all points outside the shaded area lie outside the shape, unless $d \to 0$. In the latter case $P \to X$. In other words, two third-order shock branches cannot intersect.

[9]Note, however, that the velocity of the shock can approach β_O, in which case the discontinuity in orientation becomes progressively weaker, *e.g.*, consider two circular arcs colliding and travelling over a large distance.

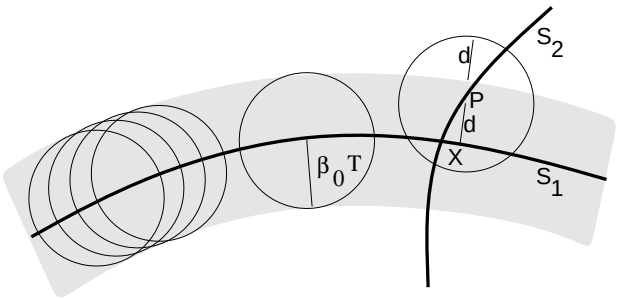

Figure 11: This figure illustrates the argument that two third-order shock branches cannot intersect. If P is a third-order shock, then all points in the circle of radius $\beta_0\mathcal{T}$ centred at P must be entirely contained in the shape. Clearly, unless $d \to 0$ this is a contradiction to the requirement (for S_1 to be a third-order shock set) that all points outside the shaded area lie outside the shape.

Proposition 7 *A first-order branch can flow into or out of a third-order branch's endpoints, but never into or out of a point that lies in the interior of a third-order branch.*

Proof: This follows from an argument similar to the one against intersecting third-order branches. Note that this is a stronger statement about the termination of a first-order shock branch in a third-order shock branch than that in Proposition 5.

Remark 2 *A single first-order branch that flows into or out of a third-order branch's endpoints, should maintain continuity of orientation.*

Explanation: This follows from fact that neither third-order nor first-order shock branches can have corners, Propositions 2 and Propositions 3. In fact third-order shocks may be viewed as limits of first-order shocks with velocity approaching infinity.

Proposition 8 *Fourth-order shocks are terminal; no shocks can flow out of them.*

Proof: This follows from the definition of a fourth-order shock; it is a point where an entire closed curve is annihilated, and hence no shocks can subsequently be born from it.

Proposition 9 *A circle is the only shape described by an isolated (fourth-order) shock. Non-circular shapes cannot have any isolated shocks.*

Proof: It is clear that a single fourth-order shock describes a circular shape. Further, by the uniqueness of the skeleton, no other shape is described by a single fourth-order shock. To see that non-circular shapes cannot have any isolated shocks, we consider each shock type in turn. By Proposition 5, a first-order shock cannot terminate unless it merges with another first-,third-, or fourth-order shock. By Remark 1, a second-order shock cannot be isolated since it always gives rise to two outward first-order shocks. A third-order shock cannot be isolated by definition. Finally, a shape cannot have two or more isolated fourth-order shocks due to the connectedness of the skeleton. Formally, let G be a connected open set in $\mathcal{R}^2$ and $r(G)$ its skeleton. Then in [43] it is proven that the adherence of its skeleton ($\overline{r}(G)$) is connected, and the mapping $G \to \overline{r}(G)$ is lower semi-continuous.

Remark 3 *For non-circular shapes, each fourth-order shock must have at least one first-order shock branch flowing into it.*

Explanation: This follows from Proposition 9 and the fact that a fourth-order shock is by definition isolated from other second-, third-, and fourth-order shocks.

Of the above constraints, those which relate to an allowed sequence of shocks in the composition of a group (the sequential constraints) can be concisely described via a shock grammar. Formally, a *grammar* G is a language generating device, which is defined by a quadruple (V, Σ, R, S) [35]. Here V is an alphabet divided into two parts, the set of *terminal* symbols $\Sigma \subseteq V$ and the set of *non-terminal* symbols $V - \Sigma$. S, the *start* symbol, is an element of $V - \Sigma$ and R, the set of *rules*, is a finite subset of $V^*(V - \Sigma)V^* \times V^*$ The grammar operates by beginning with a start symbol and then constructing a string via repeated applications of the rules. A step in the derivation involves identifying a substring in the current string which appears on the left hand side of one of the rules, and replacing it with the string that appears on the right hand side of the rule [10]. We introduce a shock grammar, SG, as follows.

Shock Grammar

- $V = \{S_1, S_2, S_{\overline{3}}, S_4, S_I, S_T, E\}$. The symbols S_1, S_2, S_4 represent first-, second-, and fourth-order shocks. Since third-order shocks never appear in isolation, a group of third-order shocks is itself an element of the alphabet, denoted by $S_{\overline{3}}$. S_I is a start symbol, S_T is a terminal symbol, and E represents the end of a growing shock sequence.
- $\Sigma = \{S_T\}$.
- $R =$

$$\begin{aligned}
&\{S_I \to S_1E, S_I \to S_2E, S_I \to S_{\overline{3}}E, S_I \to S_4,\\
&S_1E \to S_1S_1E, S_1E \to S_1S_{\overline{3}}E, S_1E \to S_4,\\
&S_2E \to S_2S_1E,\\
&S_{\overline{3}}E \to S_{\overline{3}}S_1E, S_{\overline{3}}E \to S_{\overline{3}}S_T,\\
&S_4 \to S_4S_T\}.
\end{aligned}$$

  The symbol E represents the end of a shock group that is being generated, and is used to enforce the requirement that shocks be added only to that end. This reflects the notion of time in the evolution of the shape, making the grammar context dependent.

[10] In a grammar (also called *unrestricted grammar*), the left hand sides of rules need not consist only of single non-terminals. A more restricted case is that of a *context-free grammar* where the left hand side of each rule is a single non-terminal, *i.e.*, a member of $V - \Sigma$ rather than $V^*(V - \Sigma)V^* \times V^*$.

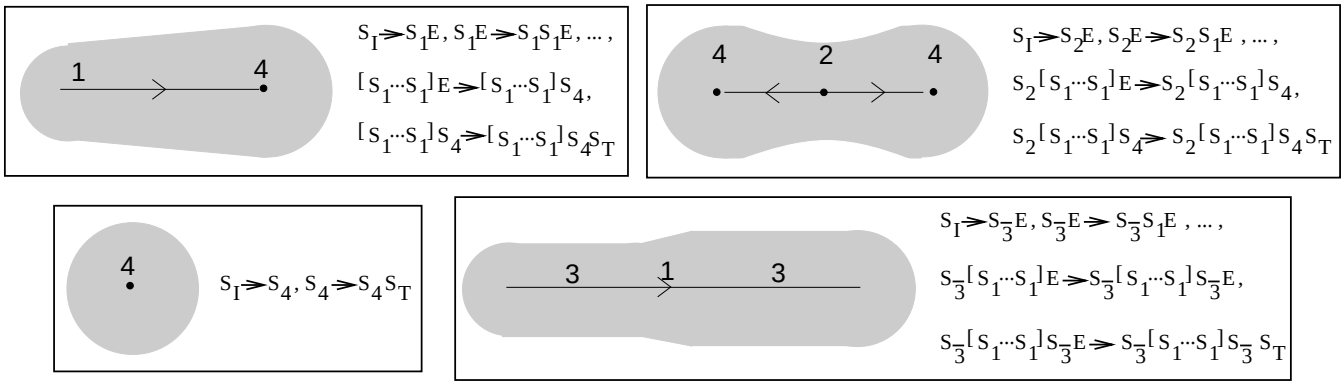

Figure 12: The examples illustrate the construction of different shock groups by repeated application of the rules of the shock grammar.

Figure 12 illustrates the application of some of the rules of SG. Note that whereas the grammar suffices to describe the composition of a shock group, it does not reflect the geometric and topological constraints discussed earlier. A possible solution may be to embed the grammar in an appropriate graph.

3.2 Pruning and Grouping

Our goal is to use the constraints on shock formation discussed above to prune impossible shock configurations, and organize shocks into more global data structures. Towards this end, in this section we outline a course of actions to be taken, with illustrative examples.

First, Propositions 1, 3, and 9 suggest a data structure of first-order shocks that have "flowed" into one another, and the following algorithm for obtaining such groups:

Action 1 *When a first-order shock is formed, it should be appended to the end of an existing first-order shock branch so long as it: 1) maintains continuity in position as well as direction of flow with the last shock added to the group, and 2) has finite speed. Otherwise, a new first-order shock branch should be initiated. Finally, if a first-order shock (or shock branch) remains isolated over a period of time, it should be annihilated.*

Next, Proposition 4 and Remark 1 suggest the following action for pruning second-order shock hypotheses:

Action 2 *A second-order shock hypothesis should be discarded if it is not initial,* i.e., *one or more first-order shock branches have flown into it, or if it does not subsequently give rise to two outward flowing first-order shock branches. Otherwise it should be kept and identified as the parent of the two first-order shock branches it gives birth to.*

Third, Proposition 7 and Remark 2 provide a further rule for pruning first-order shock hypotheses:

Action 3 *A first-order shock branch that terminates at or emanates from a point that lies in the interior of a third-order branch should be discarded. A first-order shock branch that terminates or emanates from a third-order shock branch's endpoints without maintaining continuity in orientation, should be discarded.*

Fourth, by Propositions 2, 6, and 7 third-order shock branches are smooth, and do not intersect other first-order or third-order shock branches. Therefore, it is clear that a third-order shock point has a unique orientation, provided by the orientation of the curve where opposing boundary segments have collided. Also, third order-shocks are always neighbored by other third-order shocks. This suggests a data structure for grouping together third-order shocks, and an algorithm for obtaining the groups:

Action 4 *Two third-order shock hypotheses should be grouped together if they are neighbors, and if their orientations are consistent (the shock group has to be smooth). Second, groups of third-order shocks should not intersect any other third-order or first-order shock groups. Finally, any third-order shock that remains isolated should be interpreted as a fourth-order shock.*

Finally, Propositions 8 and 9 and Remark 3 suggest the following action for interpreting fourth-order shocks:

Action 5 *A fourth-order shock hypothesis that is not isolated from other second-order, third-order, or fourth-order hypotheses should be discarded. A fourth-order shock that has no first-order branches flowing into it should be interpreted as a circle, otherwise it should be identified as the point of annihilation of the merging first-order branches.*

4 Examples

In this section we illustrate the constraints on shock formation and interaction with several examples. The results were obtained by a computer implementation of a two-stage numerical algorithm for shock classification and detection, based on the above ideas. In the figures the arrows are velocity vectors depicting the numerically computed speed and direction of flow of the last shock added to each first-order branch (Appendix B). For each example, the initial distance transform is blurred very slightly to combat noise prior to curve evolution and shock detection[11]. At every iteration shown, the subpixel outline of the evolved shape is overlayed within the pixel outline of the original. The reconstructions are simulations of the "growth" of each shape from its shock-based representation, with linear interpolation of the radius function between successive shocks on the same branch.

Figure 13 (top) illustrates the formation of shocks for a triangle shape. Under inward reaction, initially three first-order shocks are formed. Each of these flows inwards, leading to the formation of

[11]Hence the reconstructions have slightly rounded corners.

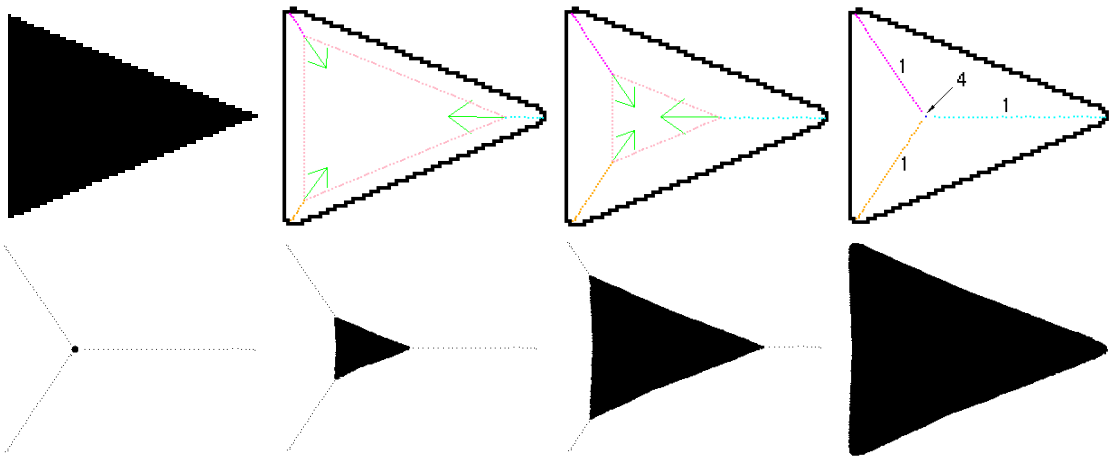

Figure 13: TOP: The formation of three first order shock branches for a triangle shape, and their termination into a single fourth order shock. The evolution of shocks under inward reaction is shown from left to right, with each distinct protrusion branch labelled. The arrows are velocity vectors depicting the speed and direction of flow of the last shock added to each branch. BOTTOM: The growth of the triangle from its shock-based description.

three *distinct* branches. The detection and grouping process for first-order shocks is robust, and, as expected, each shock branch is smooth. Eventually each branch terminates in the same fourth-order shock point, and the entire shape is annihilated. This provides a structural description of the triangle shape as a "seed" with three *distinct* "protrusions". The reconstruction of the triangle from its shock-based representation demonstrates the accuracy to which shock locations and formation times have been detected, Figure 13 (bottom).

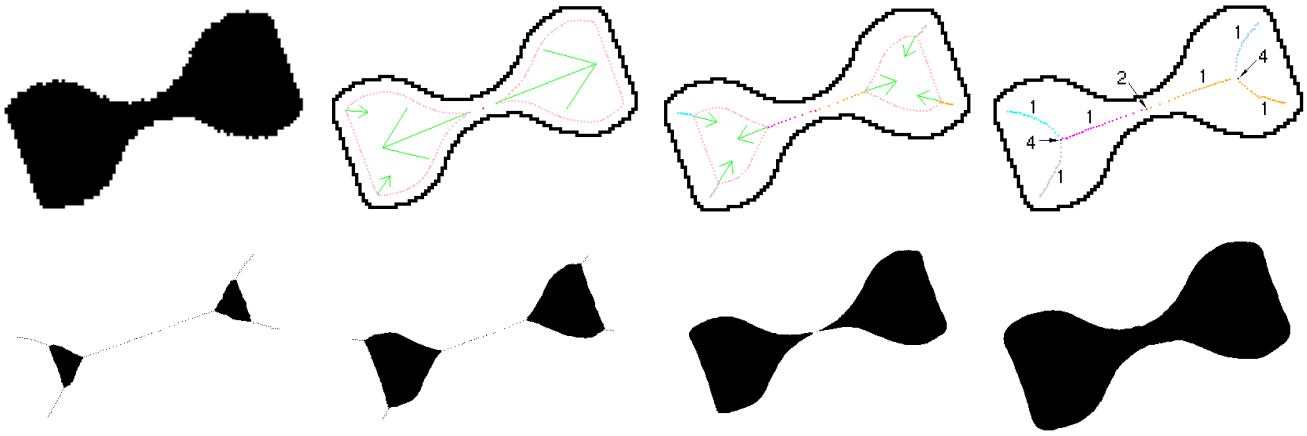

Figure 14: TOP: The evolution of shocks under inward reaction for a rotated dumbbell shape. Each distinct shock group is labelled. The arrows are velocity vectors depicting the speed and direction of flow of the last shock added to each branch. The shock-based description of the shape as a second order shock connecting two parts, each consisting of three protrusion branches emanating from a single seed, is robust to rotation. BOTTOM: The growth of the dumbbell from its shock-based description.

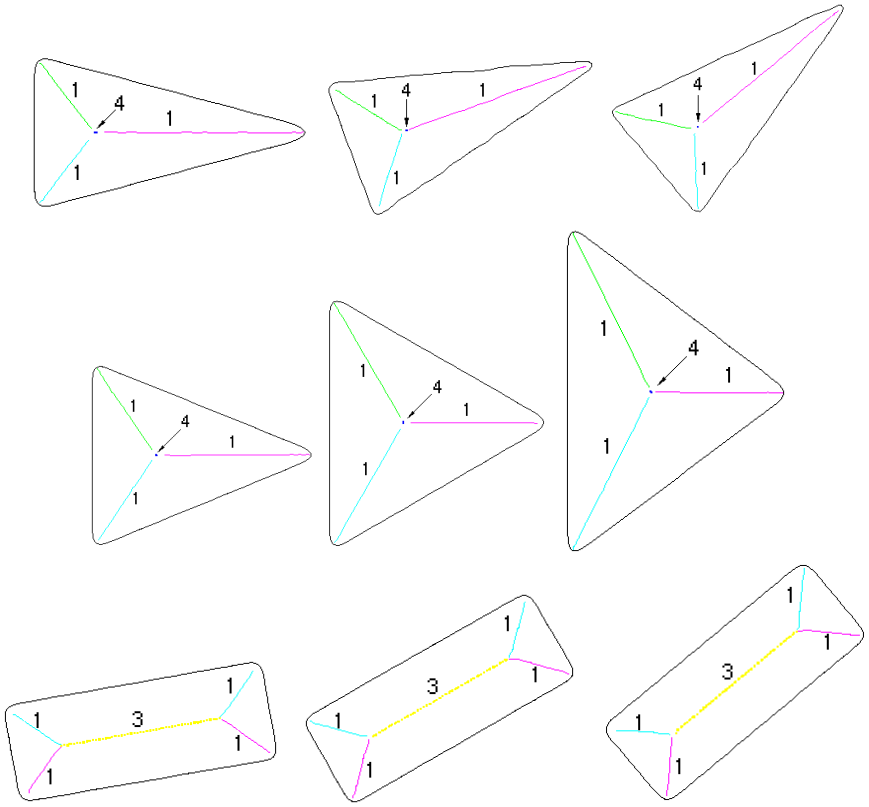

Figure 15: This figure illustrates the robustness of shock detection under rotation and stretching. The shock branches remain smooth, and no spurious branches are added. TOP: A triangle with a right vertex angle of 30 degrees is rotated in 20 degree increments. MIDDLE: The interior angle of the right vertex is increased in 15 degree increments. The structural description of each triangle emerges as "three protrusions merging into a single seed". BOTTOM: A rectangle at orientations of 10, 30 and 40 degrees is consistently described as a "bend with two protrusions at each end".

Figure 14 (top) illustrates the formation of shocks for a dumbbell shape. Under inward reaction four first-order shocks branches are formed initially. Subsequently, a second-order shock is formed at the "neck", and two additional first-order shock branches flow outwards from it. Eventually three first-order branches terminate in a single fourth-order shock, one on either side of the neck, and the entire shape is annihilated. The structural description of the shape is one of two "seed-based" parts connected by a second-order shock, where each part has three protrusions. Once again, the detection and classification process is robust for the three types of shocks present, the shock branches are smooth, and the reconstruction from shocks, Figure 14 (bottom), demonstrates the accuracy of shock detection.

Next, Figure 15 illustrates the robustness of shock detection under rotation and stretching. Whereas the shock trajectories and speeds differ in each case, the structural description of each triangle as a "single seed with three protrusions merging into it" emerges throughout. Similarly, each rectangle is described as a "bend with two protrusions" at each end. The shock branches remain smooth, and no spurious branches are added under rotation.

Figure 16 depicts the shock-based representation and reconstruction of a shape composed of trape-

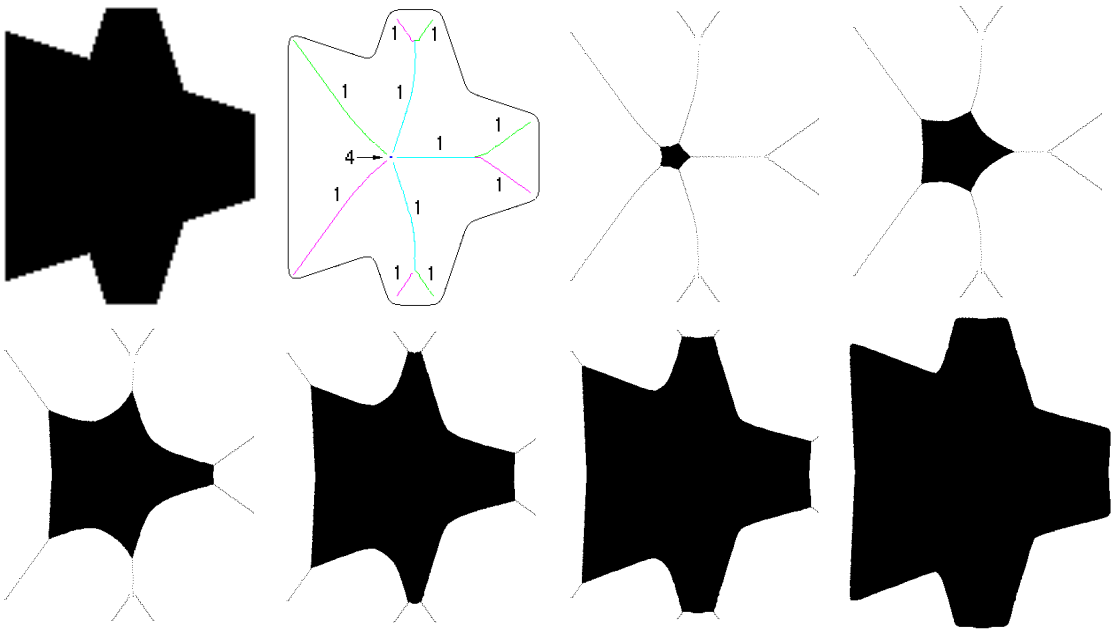

Figure 16: The shock-based description of a shape composed of trapezoids, as a hierarchy of merged protrusions, and its growth from shocks. The original shape is on the top left, and the reconstruction on the bottom right.

zoids. The description of the shape as a hierarchical collection of protrusions which eventually converge onto a single seed is intuitive and can be used for recognition.

Figure 17 depicts the shock-based representation of a biological shape, that of a hand, as a collection of bends (fingers) attached to protrusions (which describe the palm), and the growth of the shape from its shocks. Observe that the representation allows for precise reconstruction and accurate metric measurements, as well as for more qualitative perceptual classes. The latter are critical for the identification of two different shapes as instances of the same category.

Figure 18 depicts the shock-based description of two handwritten letters which have been scanned and binarized. The representation is free from artifacts of discretization, even though the resolution of the original shapes is low.

Figure 19 depicts the shock-based representation and reconstruction of a tool. Once again the description is accurate and intuitive, is robust under the movement of components, *e.g.*, the handles, and can be used for recognition. To illustrate, a different pair of pliers would match the structural description of "two large bends, attached at one end" (the handles) connected to "two smaller protrusions, also attached at one end" (the head); however the same pair of pliers would have to match relative shock locations, formation times and velocities as well.

Finally, Figure 20 illustrates the robustness of the representation in the face of occlusion, movement, and bending of parts. Observe that whereas the shock-based description is altered in the vicinity of the deformation, in remote regions, such as the palm of the hand, the representation is largely unchanged. Further, the qualitative aspects of the hand as a collection of bends attached to a central palm emerge

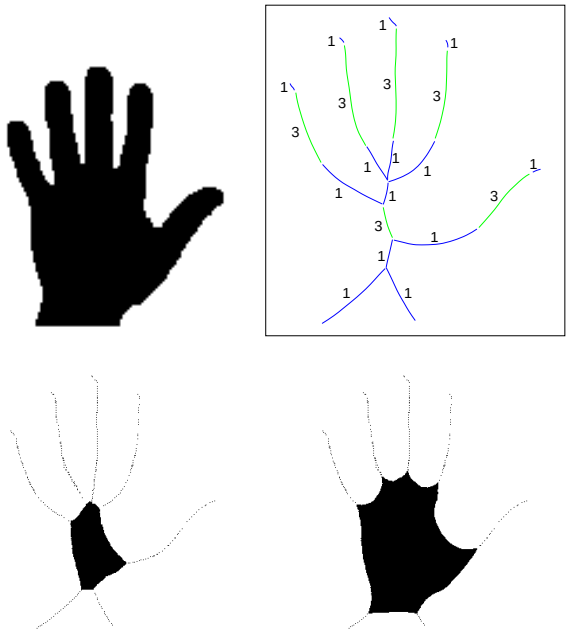

Figure 17: The shock-based description of a biological shape as five bends (the fingers) attached to protrusions (the latter describing the palm), and its growth from shocks. The original shape is on the top left, and the reconstruction on the bottom right.

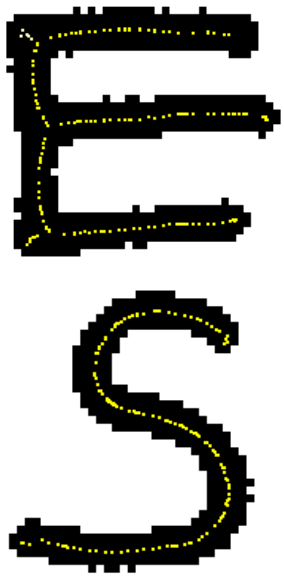

Figure 18: The shock-based description of two handwritten letters.

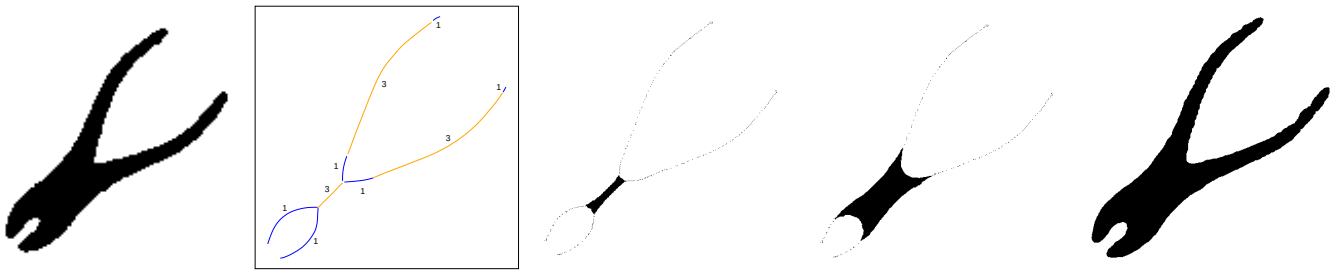

Figure 19: The shock-based description of an industrial shape, and its growth from shocks. The original shape is on the top left, and the reconstruction on the bottom right.

throughout.

5 Structural Diffusion

The set of shocks formed along the reaction axis ($\beta_1 = 0$) is equivalent to Blum's skeleton[12], Appendix A. A classical difficulty with this representation for recognition is its sensitivity to boundary

[12] Although in the case of the shock-based representation the shock points have been grouped and associated with a perceptual/semantic category.

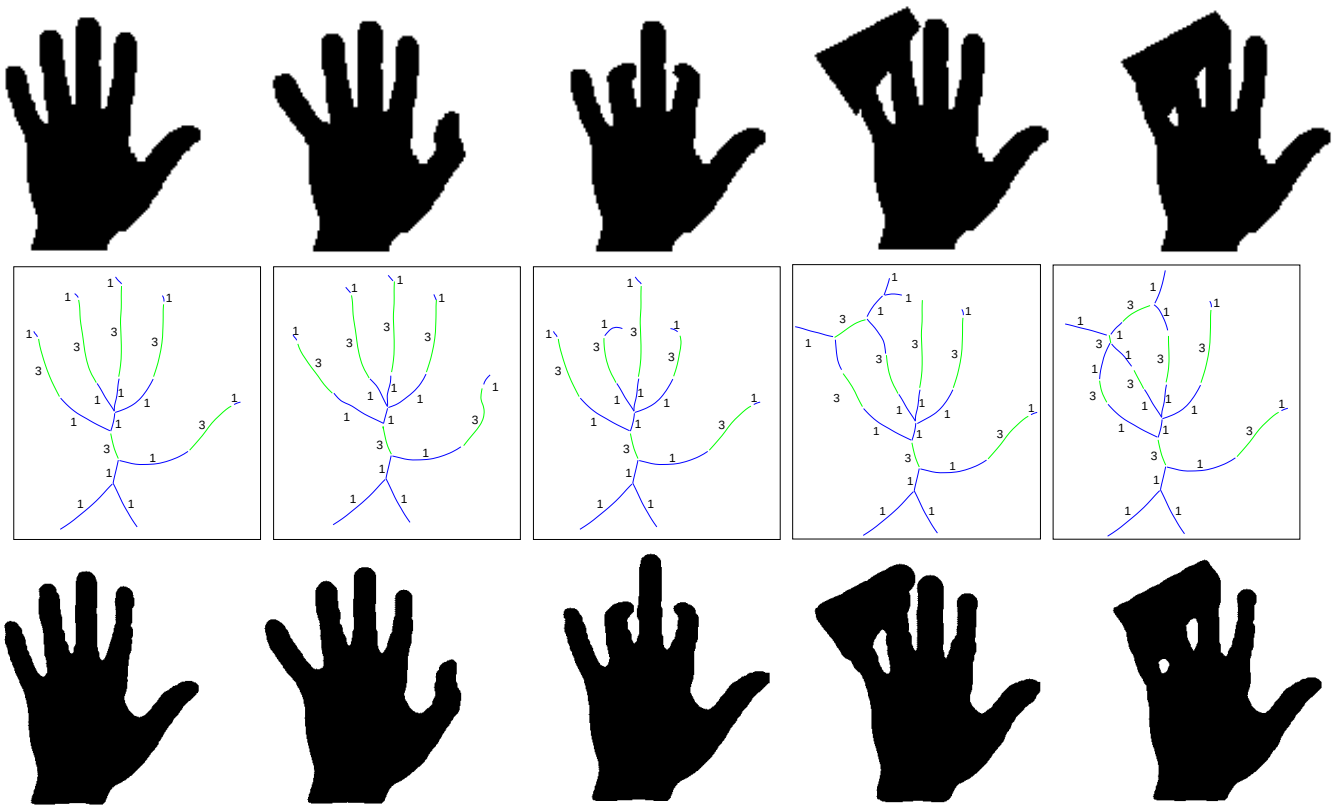

Figure 20: This Figure illustrates the robustness of the shock-based description under occlusion, and movement/bending of parts. TOP: The original shapes. MIDDLE: The shock-based description. BOTTOM: The reconstruction from shocks. Observe that a qualitative description of the shape as a collection of bends attached to a central palm emerges throughout. Further, the deformations have local effects; the precise quantitative description of remote regions, such as the palm of the hand, remains largely unchanged.

details: every positive maxima of curvature gives rise to a distinct symmetry axis [37]. In principle it is not possible to discern the significance of a branch based on its length alone and a variety of alternate measures have been proposed. Blum and Nagel suggest a *boundary axis weight*, computed as the ratio of boundary length to the length of the associated symmetric axis segment [6]. Ho and Dyer characterize the *relative prominence* of a skeletal point as the amount that the boundary segment lying between its associated bi-tangent points protrudes, with respect to the object width [21]. In a discrete implementation of the SAT based on Voronoi Diagrams [46, 47] Ogniewicz *et al.* characterize the prominence of a symmetric axis edge via the length of the associated boundary segment. In their notion of significance based on *ridge support* [36], Leymarie and Levine approximate the velocity of skeleton branch formation, integrating boundary information into the model via an initial extraction of positive maxima of curvature at which the endpoints of snakes are fixed. This allows for a multiscale approach to computing skeletons [14], and eliminates the possibility of spurious skeletal branches. A similar idea is used in [32] to obtain the skeleton, where the computation is regularized via the geomet-

ric heat equation [1, 27]. Pizer *et al.* suggest a notion of significance based on the amount of blurring required to annihilate a particular skeletal branch [52]. Upon annihilation, the branch is identified as a "child" of the branch into which it disappears, providing a hierarchical organization of SAT branches.

Whereas the above approaches often lead to intuitive results, there are potential limitations. For example, measures of prominence based solely on the length of the associated boundary protrusion [6, 46] can be very sensitive to the addition of noise to local portions of a shape, although there is little change to the shape's mass, and can require a choice of thresholds for pruning less prominent branches. On the other hand, in methods which rely on blurring the shape prior to computing its skeleton [52, 36], it is not immediately clear how skeletal branches obtained at one level of smoothing can be related to those obtained at another, in a principled fashion. Blurring the shape's region [33] can lead to topological splits, while blurring the shape's boundary can place undue emphasis on elongated features, and can lead to self-intersections[13].

Following the theoretical development of [28], the approach we suggest is to use curvature deformation (β_1) as a smoothing process to assign a significance to each shock group:

Remark 4 (Significance) *The significance of a shock group is proportional to its survival with increasing amounts of curvature deformation.*

Whereas this idea is similar in principle to Pizer *et al.*'s multiresolution SAT, the choice of curvature deformation as a smoothing process enforces a number of desirable properties[14]. In particular, in the extreme case of pure diffusion, $\frac{\beta_1}{\beta_0} \to \infty$, it is known that any embedded curve must evolve to a round point without developing self-intersections or singularities [16, 18], and that the number of extrema and inflection points is non-increasing [29]. These results imply that no new branches will form, and that the shape will disappear as a single fourth-order shock, without any other types of shock groups present. We consider the effect of diffusion on each shock type, with illustrative examples. Note that throughout, the detection of shocks with diffusion is coarse (not subpixel), and *is only intended to provide a measure of significance for shocks obtained under pure reaction.*

First-Order Shocks: In theory the slightest amount of β_1 will prevent the formation of first-order shocks altogether. Therefore, we face the dilemma that any first-order shock branches formed under pure reaction are now immediately annihilated. A practical solution is to interpret a first-order shock as a maxima of (sufficiently high) positive curvature, when $\beta_1 \neq 0$. To illustrate, Figure 21 depicts the detection of shocks for a rectangle with three triangular notches. The pure reaction evolution provides the subpixel skeleton of the shape (first column). With increasing amounts of diffusion (left to right),

[13] A potential solution is Pauwels *et al.*'s non-linear diffusion of the angle function of a closed curve, whereby boundary perturbations are suppressed while linear segments are preserved and corners are enhanced [50].

[14] It should be noted that curvature deformation is equivalent to Gaussian smoothing of the shape's boundary, provided that arc-length parametrization is preserved at each step, as in [45].

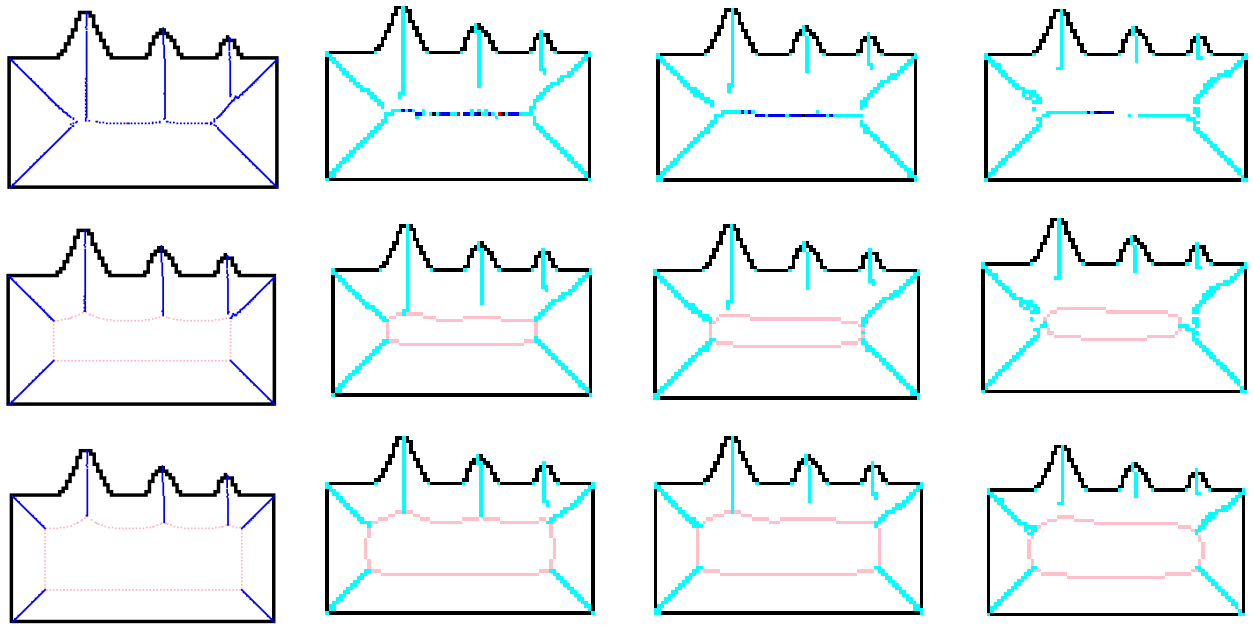

Figure 21: The survival of a first-order shock group with diffusion indicates its significance. LEFT TO RIGHT: $\beta_0 = -0.2$, $\beta_1 = 0.0, 0.125, 0.25, 0.5$. Each column depicts the shock groups that have been detected up until the present time, with the evolved shape overlayed. When $\beta_1 \neq 0$, a first-order shock is interpreted as a maxima of sufficiently high positive curvature. Observe that branches are annihilated in order of the scale of the protrusion they represent.

the survival of a group depends upon the "scale" of the corresponding protrusion [15].

Second-Order Shocks: Second-order shocks that reflect a significant narrowing of the shape will survive larger amounts of diffusion than those due to slight indentations of the boundary. To illustrate, the pure reaction description of the shape in Figure 22 is that of three seed-based parts (fourth-order shocks), with the central part connected at necks (second-order shocks) to the other two (left column). With increasing diffusion (left to right) the weaker neck is annihilated before the stronger one (right column).

Third-Order Shocks: The need for third-order shocks as a distinct category was motivated in Section 2.1. In analogy to first-order shocks, the slightest amount of β_1 will prevent the formation of third-order shocks as well. Paradoxically, under diffusion a weaker notion of third-order shocks as arising from "close to parallel" boundaries provides a categorical reference for bend-like shapes with boundary perturbations. To illustrate, the pure reaction description of the shape in Figure 23 is

[15] In discussing the lifetime in scale space as a potential measure of significance, Lindeberg has pointed out that a grey-level blob will survive longer if it is isolated from other blobs [40]. If another blob is nearby, the two may merge into a single blob, representing their union at a coarser scale. In analogy, when two protrusions are nearby the shock branches may merge into a single branch, which exists at a coarser scale (*i.e.*, it survives increasing amounts of diffusion).

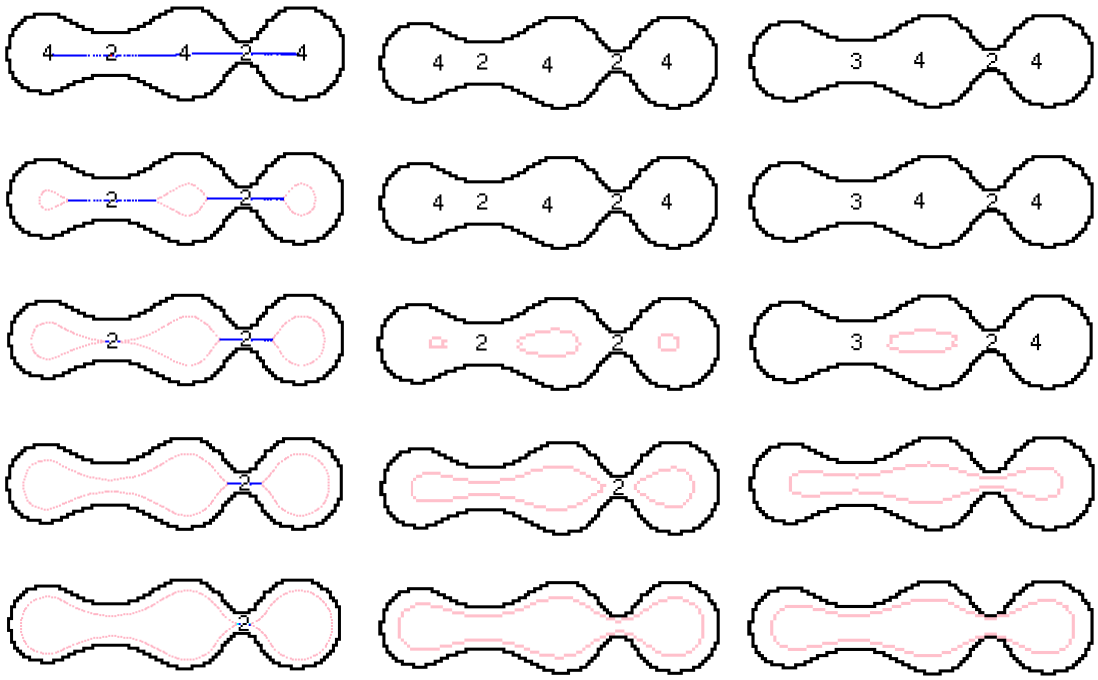

Figure 22: The survival of a second-order shock with diffusion provides a measure of its significance. LEFT TO RIGHT: $\beta_0 = -0.2$, $\beta_1 = 0.0, 1.0, 1.5$. Each column depicts shocks that have been detected up until the present time, with the evolved shape overlayed; for $\beta_1 \neq 0$ we focus on the higher-order shocks. Observe that of the two necks, the weaker one on the left is the first to annihilate with increased diffusion.

that of several seed-based parts (fourth-order shocks) with associated protrusions (first-order shocks) connected at necks (second-order shocks). With increasing diffusion (left to right), the description of the shape as a single bend (third-order shocks) emerges.

Fourth-Order Shocks: Lastly, the amount of diffusion that a fourth-order shock survives reflects the degree to which it represents a local center of mass for a shape. To illustrate, compare the rightmost fourth-order shock in Figure 22 with the leftmost one.

The notion of significance we have proposed induces a hierarchical ordering of shock branches from fine to coarse, an essential requirement for recognition. Specifically, shock branches obtained under pure reaction are removed in the order that they annihilate under diffusion, and the structures that they represent are literally broken off. To illustrate, when all shock branches are used for reconstruction, the rectangle with triangular notches is exactly obtained, Figure 24 (left). When the smallest branch (the first to annihilate under diffusion) is removed, the smallest triangle is missing in the reconstruction, Figure 24 (middle). With increased diffusion the next shock branch to annihilate represents the middle triangle, Figure 24 (right). As a second example, consider Richards' pear shapes [53], Figure 25. The shocks which survive increased diffusion bring out a coarse level similarity between the shapes as "two seed-based parts with corresponding protrusions, attached at a neck", as is reflected in the reconstructions, Figure 25 (right column).

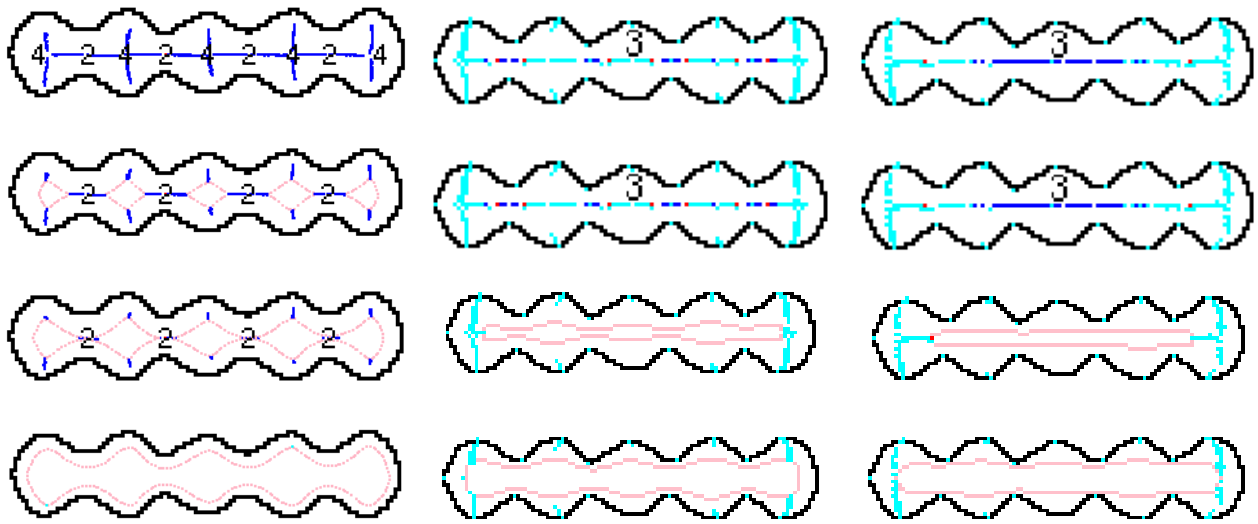

Figure 23: Diffusion regularizes bend-like shape with boundary deformations. LEFT TO RIGHT: $\beta_0 = -0.1$, $\beta_1 = 0.0, 0.25, 0.5$. Each column depicts shocks that have been detected up until the present time, with the evolved shape overlayed. Observe that with increasing diffusion, the shape is described as a single bend.

6 Shocks from Images

In conclusion, we suggest how the shock-based representation discussed in this paper can be extended to apply to fragmented shapes as they typically arise in real imagery. Specifically, whereas thus far we have assumed the availability of the shape as a starting point, it is clear that the segmentation of the shape from its background is no easy task. In the face of this difficulty, how might shock detection proceed? We speculate that the answer has to do with the interaction of local edge hypotheses, via the evolution of a local embedding surface. To illustrate, recall that in the numerical simulation of shape evolution, the choice of the distance transform as the embedding surface ϕ was made out of convenience; in fact, any Lipschitz continuous surface will suffice [15, 11]. Our proposal, therefore, is to construct a local embedding surface, by using the output of an edge operator, *i.e.*, by first placing oriented receptive fields at each local edge operator, Figure 26 (top), and then considering the covering surface, taken as the union of all such receptive fields, Figure 26 (bottom left). By construction, the covering surface has the property that its zero-crossings pass through the original edge locations. Therefore, the evolution of the covering surface can allow for the detection, classification and grouping of shocks *prior* to obtaining a segmentation of the shape itself, as depicted in Figure 26 (bottom right). In this fashion, the existence of "protrusions" and "bends" can exert a top-down influence on the figure/ground segmentation process via image evolutions along with the detection, classification and grouping of shocks.

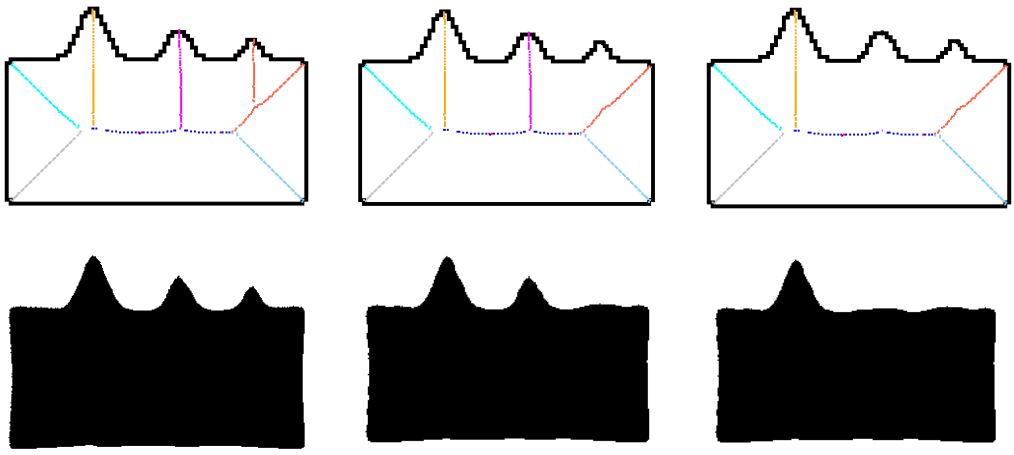

Figure 24: This figure illustrates the significance hierarchy induced by the computation in Figure 21. Top: Protrusion branches of the pure reaction description are removed in the order that they are annihilated with diffusion (left to right). Bottom: The reconstructed shapes.

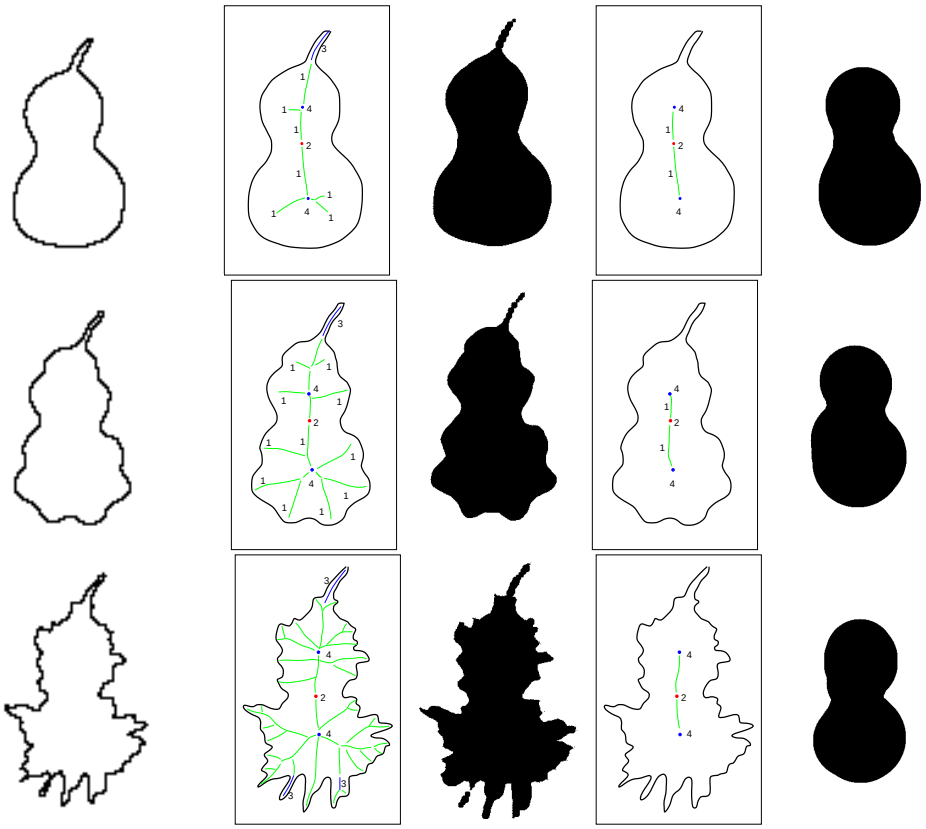

Figure 25: Column One: The original pear shapes, taken from [53]. Column Two: The shock-based description under pure reaction. Column Three: The reconstruction based on the pure reaction description (column two). Column Four: Those branches of the pure reaction description (column two) that survive under diffusion. Column Five: The reconstruction based on the description in the fourth column. Observe that a coarse level description of each pear emerges as "two seed-based parts (fourth-order shocks) attached at a neck (second-order shock)".

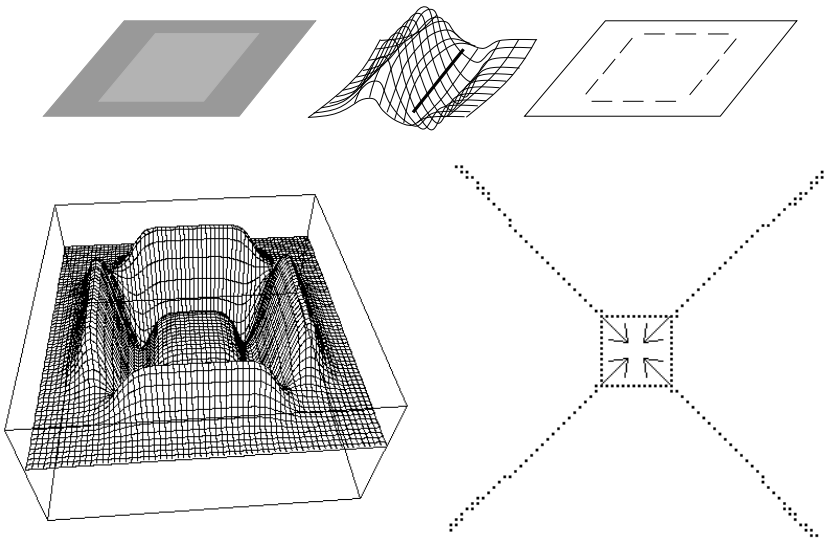

Figure 26: This figure illustrates a biologically plausible mechanism for shock detection. The original image is on the TOP LEFT. Oriented receptive fields are placed at each local edge operator, to construct a covering surface (BOTTOM LEFT). The evolution of the covering surface allows for the recovery of four protrusion branches (BOTTOM RIGHT).

A Shocks and Skeletons

The connection between shocks and Blum's skeleton [4] is given by the following theorem:

Theorem 2 *The set of shocks formed along the reaction axis of the reaction-diffusion space is equivalent to the skeleton in the sense of Blum.*

In order to proceed with the proof, we recall two important properties of the evolving front. First, the evolving front satisfies an *entropy condition* for shape [2, 56]: in the process of inward deformation, once a point is dislodged from a shape, it remains dislodged from it forever, and similarly, in the process of outward deformation, once a point becomes part of a shape, it remains part of it forever. Second, by *Hüygens' Principle*, under constant motion in the normal direction the evolved front is the envelope of circular waves issuing from the original wavefront [24].

Proof: The proof is in two stages. First, we will show that each shock point is also a skeletal point. Second, we will summarize the argument that each skeletal point is also a shock point.

To show that each shock point is a skeletal point, we must show that there exists a circle that is centered at this point, is inscribed in the shape, and is maximal. Let the shock point be formed at at t = T, and consider the circle of radius $\beta_0 T$ centered at the shock. It is clear that this circle is entirely contained in the shape, because if not, by Huygens' principle and the entropy condition it would have been dislodged from the shape's boundary before time T. We now show that the inscribed circle is also maximal for each shock type, considered in turn below.

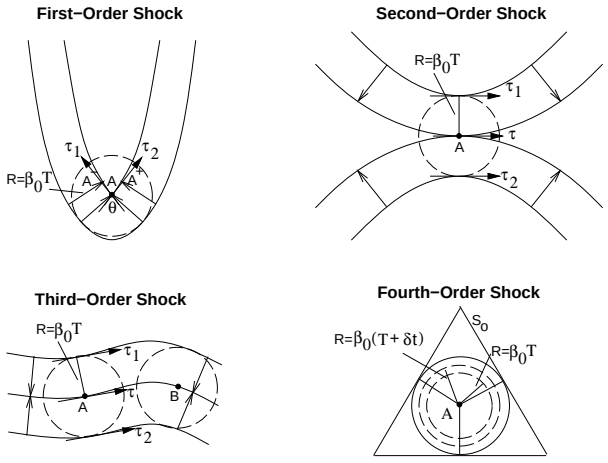

Figure 27: Under constant motion, each of the four shock types is also a skeletal point. β_0 is the amount of deformation per time step, and T is the shock's formation time.

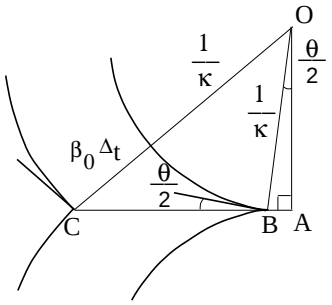

Figure 28: The computation of first-order shock speed and acceleration. The shock occurs at point B, with θ the smaller angle between the colliding boundary tangents; the boundary segments are assumed to be circular arcs with curvature κ. After one time step, the shock has moved to point C.

Let A be a *first-order* shock formed at t = T, where the boundary has an orientation discontinuity, (see Figure 27). Since characteristics push *into* a shock, the angle θ between the boundary tangents τ_1, and τ_2 must be smaller than π. Points infinitesimally close to $\mathcal{A}$ along the boundary, $\mathcal{A}^+$ and $\mathcal{A}^-$, can be exactly traced back to the original boundary. Note that since $\frac{\partial \vec{N}}{\partial t} = 0$ along the reaction axis [29], the point on the original boundary giving rise to $\mathcal{A}^-$ is $\beta_0 T$ away from it. Therefore, the left and right boundaries of the deformed shape are parallel to the original boundary, and $\beta_0 T$ away. Further, since the circle of radius $\beta_0 T$ is entirely contained in the shape, the circle must be tangent tangent to the reconstructed original boundary. No points of the original shape are inside this circle, since by *Hüygens' Principle* and the entropy condition, point A would have disappeared before time T. Therefore, the circle with radius $\beta_0 T$ and center A is the maximal circle that can be inscribed, and A is a skeletal point.

Next, let A be a *second-order* shock formed at time t = T. From Theorem 1, the colliding boundary points have parallel tangents. Since $\frac{\partial \vec{T}}{\partial t} = 0$, the corresponding points at the originating boundary segments have parallel tangents as well (if they exist). As such, a circle with radius $\beta_0 T$ and center A is tangent to these boundary points, and is also maximal (by *Hüygens' Principle* and the entropy condition). Therefore, A is a skeletal point.

Since *third-order* shocks satisfy the properties of second order shocks, except they are not isolated, the above argument holds for third order shocks as well.

Finally, let A be a *fourth-order* shock at time t = T, which is formed when the entire boundary collapses into that point. A circle of radius $\beta_0 T$ and center A must be tangent to the original boundary at at least two points. Suppose to the contrary we assume that the circle with radius $\beta_0 T$ is entirely embedded in the shape. Then $\exists\ \delta\tau <$ min distance(S_o, circle), such that the circle with radius $R = (\beta_0 T + \delta\tau)$ is entirely embedded in the original shape. If $\mathcal{C}_o$ and $\hat{\mathcal{C}}_o$ are two compact subsets of

$\mathbf{R^2}$ such that $\mathcal{C}_o \subseteq \hat{\mathcal{C}}_o$ then the subsequent evolutions $\mathcal{C}_t$ and $\hat{\mathcal{C}}_t$ of $\mathcal{C}_o$ and $\hat{\mathcal{C}}_o$, by (2) satisfy $\mathcal{C}_t \subseteq \hat{\mathcal{C}}_t$ [11]. Therefore, taking the circle of radius $(\beta_0 T + \delta\tau)$ and the original shape as $\mathcal{C}_o$ and $\hat{\mathcal{C}}_o$ respectively, it is clear that shock point A would not have formed at time t = T, a contradiction. Therefore, the circle wxith radius $\beta_0 T$ and centered at A is maximal, and A is a skeletal point. This completes the proof that all shock points are also skeletal points.

The second part of the argument, that every skeletal point is a shock, has been summarized in Section 2.1. Let the maximal disc centered at the skeletal point have radius R, and associated bi-tangent points with the shape; the shock's formation time is obtained from $R = \beta_0 T$, and its type depends on the boundary tangents and boundary segments at the bi-tangent points, Figure 4.

B Shock Speed and Acceleration

Let a first-order shock occur at point B, let the smaller angle between the boundary tangents be θ, and let each boundary segment be a circular arc with curvature κ, Figure 28. Let the shape's boundary be deformed by a constant motion $\beta_0 \Delta t$ in the normal direction.

With $AB = \kappa^{-1} sin(\theta/2)$, the speed of the shock is $AB' = (\kappa^{-1})' sin(\theta/2) + \frac{1}{2\kappa} cos(\theta/2)\theta'$.
Using the relations $OA = \kappa^{-1} cos(\theta/2), OA' = (\kappa^{-1})' cos(\theta/2) - \frac{1}{2\kappa} sin(\theta/2)\theta' = 0$,
$(\kappa^{-1})' = lim_{\Delta t \to 0} \frac{\beta_0 \Delta t}{\Delta t} = \beta_0$; θ' is seen to be $\frac{2\beta_0 \kappa}{tan(\theta/2)}$.
Substituting for θ', the **speed** is given by $\boxed{\beta_0 (sin(\theta/2) + \frac{cos^2(\theta/2)}{sin\theta/2}) = \frac{\beta_0}{sin(\theta/2)}.}$

The acceleration of the shock is obtained by differentiating the speed: $-\beta_0 cos(\theta/2)\theta'/2sin^2(\theta/2)$.
Substituting for θ' , the acceleration is seen to be: $-\beta_0^2 cos^2(\theta/2)\kappa/sin^3\theta/2$.
From the derived expression for speed we have the relations $sin(\theta/2) = \beta_0/s$; $cos^2(\theta/2) = 1 - \beta_0^2/s^2$.
Hence, the **acceleration** can be expressed as $\boxed{a = \frac{s(\beta_0^2 - s^2)\kappa}{\beta_0}.}$

Finally, the **derivative of boundary curvature** is given by $\boxed{\kappa' = ((\kappa^{-1})^{-1})' = -\kappa^2 (\kappa^{-1})' = -\beta_0 \kappa^2.}$

Acknowledgements The support of NSF grant IRI-9305630 is gratefully acknowledged. We thank Jonas August, Michael Kelly, Eric Pauwels, and Steve Zucker for helpful discussions.

References

[1] L. Alvarez, P.-L. Lions, and J.-M. Morel. Image selective smoothing and edge detection by nonlinear diffusion: II. *SIAM Journal of Numerical Analysis*, 29(3):845–866, June 1992.

[2] G. Barles. Remarks on a flame propagation model. Technical Report No 464, INRIA Rapports de Recherche, December 1985.

[3] I. Biederman. Recognition by components. *Psych. Review*, 94:115–147, 1987.

[4] H. Blum. Biological shape and visual science. *J. Theor. Biol.*, 38:205–287, 1973.

[5] H. Blum. A geometry for biology. *Annals of N.Y. academy of Sciences, Mathematical Analysis of Fundamental Biological Phenomena*, 213:19–30, 1974.

[6] H. Blum and R. N. Nagel. Shape description using weighted symmetric axis features. *Pattern Recognition*, 10:167–180, 1978.

[7] M. Brady and H. Asada. Smoothed local symmetries and their implementation. *International Journal of Robotics Research*, 3(3), 1984.

[8] J. Bruce and P. Giblin. *Curves and Singularities*. Cambridge University Press, 1984.

[9] J. W. Bruce, P. J. Giblin, and C. G. Gibson. Symmetry sets. *Proceedings of the Royal Society of Edinburgh*, 101A:163–186, 1985.

[10] C. A. Burbeck and S. M. Pizer. Object representation by cores: Identifying and representing primitive spatial regions. *Vision Research*, 1994.

[11] Y. Chen, Y. Giga, and S. Goto. Uniqueness and existence of viscosity solutions of generalized mean curvature flow equations. *Journal of Differential Geometry*, 33(3):749–786, 1991.

[12] M. G. Crandall, H. Ishii, and P.-L. Lions. User's guide to viscosity solutions of second order partial differential equations. *Bulletin of the American Mathematical Society*, 27(1):1–67, 1992.

[13] R. Deriche and G. Giraudon. Accurate corner detection: An analytical study. In *The Proceedings of Third International Conference on Computer Vision*, pages 66–70, Osaka, Japan, December 1990. IEEE Computer Society Press.

[14] A. R. Dill, M. D. Levine, and P. B. Noble. Multiple resolution skeletons. *IEEE PAMI*, 9(4):495–504, July 1987.

[15] L. C. Evans and J. Spruck. Motion of level sets by mean curvature I. *Journal of Differential Geometry*, 33(3):635–681, May 1991.

[16] M. Gage and R. S. Hamilton. The heat equation shrinking convex plane curves. *J. Differential Geometry*, 23:69–96, 1986.

[17] P. J. Giblin and S. A. Brassett. Local symmetry of plane curves. *The American Mathematical Monthly*, 92:689–707, December 1985.

[18] M. A. Grayson. The heat equation shrinks embedded plane curves to round points. *J. Differential Geometry*, 26:285–314, 1987.

[19] A. Harten. ENO schemes with subcell resolution. *Journal of Computational Physics*, 83:148–184, 1989.

[20] A. Harten, B. Engquist, and R. Sukumar. Uniformly high order accurate essentially non-oscillatory schemes, III. *Journal of Computational Physics*, 71:231–303, 1987.

[21] S.-B. Ho and C. R. Dyer. Shape smoothing using medial axis properties. *IEEE PAMI*, 8(4):512–520, July 1986.

[22] D. D. Hoffman and W. A. Richards. Parts of recognition. *Cognition*, 18:65–96, 1985.

[23] L. A. Iverson and S. W. Zucker. Logical/linear operators for image curves. *IEEE PAMI*, 1995.

[24] F. John. *Partial Differential Equations*. Springer-Verlag, 1971.

[25] M. Kelly and M. D. Levine. Annular symmetry operators: A method for locating and describing objects. In *Fifth International Conference on Computer Vision*, pages 1016–1021, Boston, Massachusetts, June 1995. IEEE Computer Society.

[26] B. B. Kimia. Conservation laws and a theory of shape. Ph.D. dissertation, McGill Centre for Intelligent Machines, McGill University, Montreal, Canada, 1990.

[27] B. B. Kimia and K. Siddiqi. Geometric heat equation and non-linear diffusion of shapes and images. In *CVPR'94 (IEEE Computer Society Conference on Computer Vision and Pattern Recognition, Seattle, Washington, June 21–23, 1994)*, Washington, DC., June 1994. Computer Society Press.

[28] B. B. Kimia, A. R. Tannenbaum, and S. W. Zucker. Toward a computational theory of shape: An overview. In *Proceedings of the First European Conference on Computer Vision*, Antibes, France, 1990. Springer Verlag.

[29] B. B. Kimia, A. R. Tannenbaum, and S. W. Zucker. On the evolution of curves via a function of curvature, I: The classical case. *JMAA*, 163(2), January 1992.

[30] B. B. Kimia, A. R. Tannenbaum, and S. W. Zucker. The shape triangle: Parts, protrusions, and bends. In *Proceedings of the International Workshop on Visual Form*, pages 307–323, Capri, Italy, May 1994. World Scientific.

[31] B. B. Kimia, A. R. Tannenbaum, and S. W. Zucker. Shapes, shocks, and deformations, I: The components of shape and the reaction-diffusion space. *International Journal of Computer Vision*, 15:189–224, 1995.

[32] R. Kimmel, D. Shaked, N. Kiryati, and A. M. Bruckstein. Skeletonization via distance from boundary and the zero sets approach. In *Proceedings SPIE - Geometric Methods in Computer Vision III, Boston, MA*, November 1994.

[33] J. J. Koenderink and A. J. van Doorn. Dynamic shape. *Biological Cybernetics*, 53:383–396, 1986.

[34] P. D. Lax. *Shock Waves and Entropy*, pages 603–634. Academic Press, New York, 1971.

[35] H. Lewis and C. Papadimitriou. *Elements of the Theory of Computation.* Prentice-Hall, 1981.

[36] F. Leymarie and M. D. Levine. Simulating the grassfire transform using an active contour model. *IEEE PAMI*, 14(1):56–75, January 1992.

[37] M. Leyton. Symmetry-curvature duality. *Computer Vision, Graphics, and Image processing*, 38:327–341, 1987.

[38] M. Leyton. A process grammar for shape. *Artificial Intelligence*, 34:213–247, 1988.

[39] M. Leyton. *Symmetry, Causality, Mind.* MIT press, April 1992.

[40] T. Lindeberg. *Scale-Space Theory In Computer Vision.* Kluwer Academic Publishers, 1994.

[41] P. Lions. *Generalized Solutions of Hamilton Jacobi Eqautions.* Pitman, 1981.

[42] D. Marr and K. H. Nishihara. Representation and recognition of the spatial organization of three dimensional structure. *Proceedings of the Royal Society of London*, B 200:269–294, 1978.

[43] G. Matheron. Examples of topological properties of skeletons. In Serra [55], pages 217–238.

[44] F. Meyer. Skeletons in digital spaces. In Serra [55], pages 257–296.

[45] F. Mokhtarian and A. Mackworth. A theory of multiscale, curvature-based shape representation for planar curves. *PAMI*, 14(8):789–805, August 1992.

[46] R. L. Ogniewicz. *Discrete Voronoi Skeletons.* Hartung-Gorre, 1993.

[47] R. L. Ogniewicz and O. Kübler. Hierarchic voronoi skeletons. Technical Report BIWI-TR-145, Communication Technology Laboratory, ETH Zürich, July 1993.

[48] S. Osher and J. Sethian. Fronts propagating with curvature dependent speed: Algorithms based on Hamilton-Jacobi formulations. *Journal of Computational Physics*, 79:12–49, 1988.

[49] P. Parent and S. W. Zucker. Trace inference, curvature consistency and curve detection. *IEEE PAMI*, 11(8):823–839, August 1989.

[50] E. J. Pauwels, P. Fiddelaers, and L. J. V. Gool. Geometry-driven evolution and functional optimization for curves. Technical Report KUL/ESAT/MI2/9414A, Katholieke Universiteit Leuven, Belgium, November 1994.

[51] S. M. Pizer, S. Murthy, and D. T. Chen. Core-based boundary claiming. volume 2167, pages 151–159. SPIE, 1994.

[52] S. M. Pizer, W. R. Oliver, and S. H. Bloomberg. Hierarchical shape description via the multiresolution symmetric axis transform. *IEEE PAMI*, 9(4):505–511, 1987.

[53] W. Richards, B. Dawson, and D. Whittington. Encoding contour shape by curvature extrema. *Journal of Optical Society of America*, 3(9):1483–1489, 1986.

[54] G. L. Scott, S. Turner, and A. Zisserman. Using a mixed wave/diffusion process to elicit the symmetry set. *Image and Vision Computing*, 7(1):63–70, February 1989.

[55] J. Serra, editor. *Image Analysis and Mathematical Morpholpogy, Part II: Theoretical Advances*. Academic Press, 1988.

[56] J. A. Sethian. Curvature and the evolution of fronts. *Comm. Math. Physics*, 101:487–499, 1985.

[57] C.-W. Shu and S. Osher. Efficient implementation of essentially non-oscillatory shock-capturing schemes. *Journal of Computational Physics*, 77:439–471, 1988.

[58] K. Siddiqi, B. B. Kimia, and C. Shu. Geometric shock-capturing eno schemes for subpixel interpolation, computation and curve evolution. In *International Symposium on Computer Vision*, Coral Gables, Florida, November 1995. IEEE Computer Society.

[59] B. Vaselle, G. Giraudon, and M. Berthod. Following corners on curves and surfaces in scale space. In J.-O. Eklundh, editor, *Proceedings of the Third European Conference on Computer Vision*, Stockholm, 1994. Springer Verlag.

[60] S. W. Zucker, A. Dobbins, and L. Iverson. Two stages of curve detection suggest two styles of visual computation. *Neural Computation*, 1:68–81, 1989.